Title

Sterile liver injury induces a protective tissue-resident cDC1-ILC1 circuit through cDC1-intrinsic cGAS-STING-dependent IL-12 production.

Journal

Cell Reports, 42(2)

Authors

Hildreth, Andrew
Padilla, Eddie
Tafti, Rana
et al.

Publication Date

2023-02-28

DOI

10.1016/j.celrep.2023.112141

Peer reviewed

HHS Public Access

Author manuscript

Cell Rep. Author manuscript; available in PMC 2023 October 23.

Published in final edited form as:

Cell Rep. 2023 February 28; 42(2): 112141. doi:10.1016/j.celrep.2023.112141.

Sterile liver injury induces a protective tissue-resident cDC1-ILC1 circuit through cDC1-intrinsic cGAS-STING-dependent IL-12 production

Andrew D. Hildreth[1,2], **Eddie T. Padilla**[1], **Rana Yakhshi Tafti**[1], **Akshara R. Legala**[1], **Timothy E. O'Sullivan**[1,2,3,*]

[1]Department of Microbiology, Immunology, and Molecular Genetics, David Geffen School of Medicine at UCLA, Los Angeles, CA 90095, USA

[2]Molecular Biology Institute, University of California, Los Angeles, Los Angeles, CA 90095, USA

[3]Lead contact

SUMMARY

Tissue-resident immune cells are critical to the initiation and potentiation of inflammation. However, the tissue-protective cellular communication networks initiated by resident immunity during sterile inflammation are not well understood. Using single-cell transcriptomic analysis, we show the liver-resident cell connectome and signalome during acute liver injury. These analyses identify *Il12b* as a central regulator of liver injury-associated changes in gene expression. Interleukin (IL)-12 produced by conventional type 1 dendritic cells (cDC1s) is required for protection during acute injury through activation of interferon (IFN)-γ production by liver-resident type 1 innate lymphoid cells (ILC1s). Using a targeted *in vivo* CRISPR-Cas9 screen of innate immune sensing pathways, we find that cDC1-intrinsic cGAS-STING signaling acts upstream of IL-12 production to initiate early protective immune responses. Our study identifies the core communication hubs initiated by tissue-resident innate immune cells during sterile inflammation *in vivo* and implicates cDC1-derived IL-12 as an important regulator of this process.

Graphical Abstract

*Correspondence: tosullivan@mednet.ucla.edu.

AUTHOR CONTRIBUTIONS

A.D.H. and T.E.O. designed the study; A.D.H., E.T.P., R.Y.T., and A.R.L. performed the experiments; R.Y.T. and E.T.P. performed bioinformatics analyses; T.E.O. and A.D.H. wrote the manuscript.

SUPPLEMENTAL INFORMATION

Supplemental information can be found online at https://doi.org/10.1016/j.celrep.2023.112141.

DECLARATION OF INTERESTS

T.E.O is an advisory board member for Modulus Therapeutics and Xyphos, Inc.

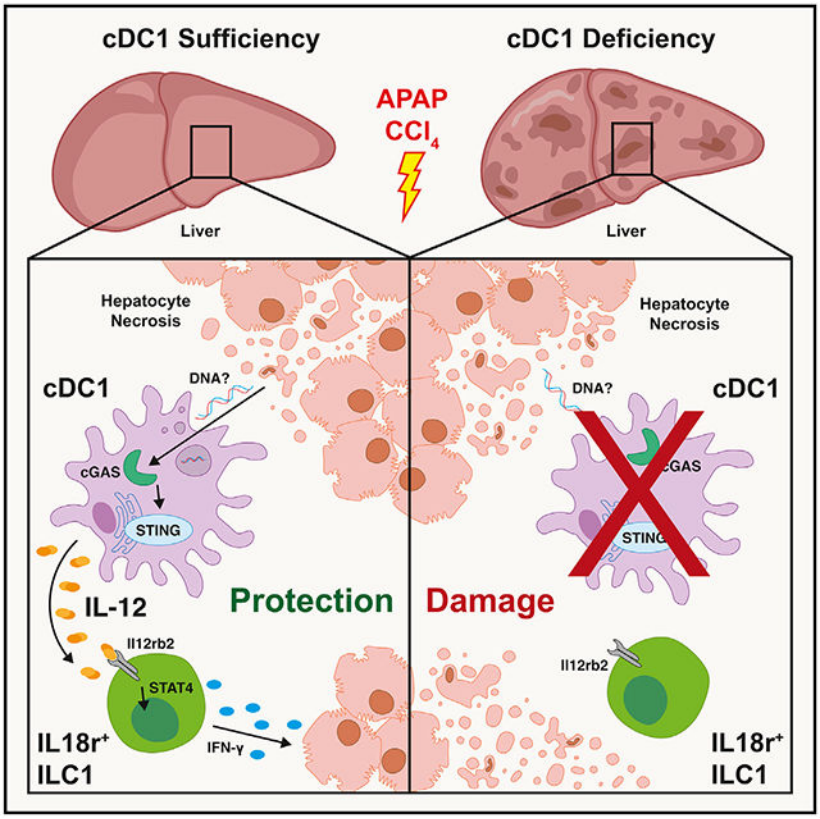

In brief

Hildreth et al. identify conventional type 1 dendritic cells (cDC1s) and interleukin (IL)-12 as critical regulators of sterile inflammation during acute liver injury. cDC1-intrinsic cGAS-STING signaling induces IL-12 to activate protective circuits including IFN-γ production by liver-resident type 1 innate lymphoid cells (ILC1s).

INTRODUCTION

Tissue-resident innate immune cells initiate inflammation and immune responses involved in the clearance of pathogens and wound healing.[1] In the absence of pathogen-associated molecular patterns, tissue-resident immunity can be activated during trauma, drug-induced injury, and anti-tumor responses to induce sterile inflammation.[2–4] However, the cellular communication networks of tissue-resident immune cells that coordinate and initiate sterile inflammatory responses are not well understood. While inflammation is critical to injury resolution, sustained immune activation can lead to disease progression and fibrosis.[5,6] Thus, understanding the cell types and molecular mechanisms that drive sterile inflammation in these contexts is critical to the development of treatment strategies for both acute and chronic disease.

Acetaminophen (APAP) toxicity is the leading cause of acute liver failure in the United States.[7] Acute APAP overdose leads to the formation of noxious metabolites, which cause cell death and hepatocyte necrosis, inducing sterile inflammation.[8] Previous studies

have implicated liver-resident Kupffer cells, recruited macrophages, and neutrophils in the initiation and potentiation of sterile liver inflammation.[4,8] However, recent single-cell RNA sequencing (scRNA-seq) studies have begun to appreciate the extent of the cellular heterogeneity present within the liver as well as the potential of previously overlooked cell types to contribute to the kinetic and spatial regulation of sterile inflammation.[9–13] While cutting-edge methods to assess cellular communication networks have identified critical mediators of sterile inflammation during chronic nonalcoholic steatohepatitis (NASH)-associated fibrotic responses,[14,15] an unbiased analysis of liver-resident immune cell activation states and communication networks that contribute to the initiation of acute sterile liver inflammation has not been performed.

Here, we utilized a mouse APAP overdose acute liver injury scRNA-seq dataset to uncover the liver-resident immune cell types and interactions that regulate early sterile inflammation. We showed that tissue-resident activated Kupffer cells and conventional type 1 dendritic cells (cDC1s), in addition to liver-infiltrating monocytes and lipid-associated macrophages (LAMs), act as core regulators of liver injury-associated changes in gene expression. Unbiased analysis of cellular communication networks using connectome and signalome analysis highlighted the importance of *Il12b* from activated cDC1s as a key driver of sterile inflammation during liver injury. cDC1-derived interleukin (IL)-12 was required for protective responses during acute liver injury through induction of interferon (IFN)-γ production by liver-resident type 1 innate lymphoid cells (ILC1s). Furthermore, using a targeted *in vivo* CRISPR-Cas9 screen of innate immune sensing pathways validated by knockout mice, we identified cGAS-STING upstream of IL-12 production by cDC1s as critical for initiation of early protective responses. Together, our results implicate liver cDC1s as important mediators of protective sterile inflammation.

RESULTS

scRNA-seq analysis of acute liver injury identifies early activation states of liver-resident immune cells

To gain an unbiased understanding of the tissue-resident immune response immediately following sterile tissue injury, we analyzed a publicly available scRNA-seq dataset derived from mouse liver cells harvested from wild-type (WT) or 24 h post-high-dose-APAP-injected mice.[10] The resulting quality-controlled single-cell atlas included 2,558 cells that were clustered based on differential expression of marker genes and visualized using a uniform manifold approximation and projection (UMAP) plot (Figures 1A and S1A; Table S1). Clustering analysis revealed 24 distinct clusters including naive $CD4^+$ and $CD8^+$ T cells, regulatory T cells (Tregs), activated $CD8^+$ T cells, γδ T cells (γδTs), IFN-stimulated T cells, ILC1s, natural killer (NK) cells, cDC1s, plasmacytoid DCs (pDCs), monocytes, LAMs, Kupffer cells (KCs), B cells, hepatic-stellate cells (HSCs), endothelial cells, cholangiocytes (Chols), and hepatocytes. While identified nonimmune and lymphoid clusters contained cells from both APAP-treated and WT mice, several myeloid populations, including activated cDC1s (*Ccr7*, *Fscn1*, *Il15ra*, *Mreg*), activated KCs (*Mmp12*, *Mmp13*, *Marco*), LAMs (*Cd63*, *Trem2*, *Cd9*, *Lgals3*), and monocytes (*Cx3cr1*, *Ccr2*, *S100a4*) were enriched 24 h following APAP treatment (Figures 1B, 1C, and S1A; Table S1). To

validate these findings, we treated an additional cohort of mice with APAP to induce acute liver injury and assessed the accumulation of these populations within the liver 24 h post-treatment via flow cytometry. Compared with WT controls, we found increased LAM, transitioning monocyte, and Ly6C$^+$ monocyte population numbers and frequencies as a percentage of total CD45$^+$ cells (Figures 1D, 1E, and S1B), which is consistent with previous studies reporting the accumulation of recruited monocyte and macrophage populations in the liver during injury.[15–17] Neutrophils have also been shown to be recruited to the liver during injury,[18,19] which we validated with our flow cytometry cohort (Figures S1B and S1C). However, this population was not present in the analyzed scRNA-seq dataset. Although the frequency of Ly6C$^-$ monocytes was increased in injured mice, no changes in the number or frequency of Ly6C$^-$ monocytes, peritoneal macrophages, or KCs were observed (Figures S1B–S1D). We also found that cDC2, cDC1, and activated cDC1 population numbers and frequencies were increased within APAP-treated mice (Figures 1F and S1E), suggesting a potential previously unrecognized role for tissue-resident DCs during acute sterile liver injury.

Single-cell receptor-ligand analysis reveals transcriptional regulators during liver injury

We next analyzed how liver cellular communication networks changed following acute liver injury. Using CellChat receptor-ligand analysis,[20] we visualized the putative aggregated cellular communication networks from both WT and APAP-treated groups of cells and weighted for the top 25% of interactions (Figures S2A and S2B; Table S2, S3, S4, and S5). This analysis highlighted major paracrine signaling networks from KCs, HSCs, endothelial cells, and Chols to both lymphoid (T cell subsets, ILC1s, and NK cells) and myeloid (cDC1s, pDCs, and monocytes) subsets in the WT liver (Figure S2A). In contrast, putative paracrine interactions stemming from monocytes, LAMs, activated KCs, cDC1s, activated cDC1s, hepatocytes, and Chols to T cells (IFN stimulated and immature) as well as cDC1s were enriched within the APAP-treated liver (Figures 2A–2D and S2B). Putative autocrine interactions in monocytes, LAMs, and activated KCs were also considerably enriched within the APAP-treated liver dataset. Together, these data suggest a dramatic shift from nonimmune to innate immune populations as central communicators during sterile liver injury.

To better understand the potential impact of these cell types on driving the tissue-resident immune response to sterile liver injury, we utilized NicheNet[21] to determine whether putative signals from APAP-enriched communicating cell types may be upstream of APAP-induced transcriptional changes in other cell types. NicheNet identified 20 putative regulators of gene expression in various cell types (Figure 2E; Table S6). Of these, 14 were expressed in APAP-enriched populations including activated cDC1s (*Icam1*, *Il12b*, *Nectin1*, *H2.M3*, *Cd40*), activated KCs and KCs (*Icam1*, *Il1a*, *Mmp13*, *H2.M3*, *Hbegf*, *Il18*), and LAMs (*Sema4d*, *Ccl2*, *Ccl12*, *Ccl7*, *Ccl3*) (Figures 2E and S2C). To further assess how these cell types may be regulating downstream gene expression changes within the liver injury landscape, we analyzed the top 25% of the interaction scores between each of these key regulators and their top 50 most strongly predicted gene targets (Figure 2E; Table S7). While many key regulators had overlapping active target genes, *Ccl12*, *Ccl2*, *Mmp13*, and *Il12b* had increased average regulatory potential among the shared downstream target genes.

These results suggested that LAMs, activated KCs, and activated cDC1s act as key drivers of gene expression changes in other cell types 24 h following sterile liver injury *in silico*.

To determine the specific gene expression changes in cell types downstream of these regulatory signals, we assessed the number of direct signaling interactions between LAMs, activated KCs, activated cDC1s, and other cell types (Figures 2F, S2D, and S2El; Table S7). We identified a total of 159 putative interactions derived from these three populations (LAMs: 84, activated KCs: 42, and activated cDC1s: 33) and were able to validate the expression of the majority of NicheNet's suggested target genes within identified cell types present in this dataset. Through *Ccl2*, *Ccl12*, and *Ccl7*, LAMs were identified as upstream of putative interactions involving 23 cell types via *Ccr2* and *Ackr2* (Figure S2D). Analysis of these target genes suggested that LAMs may regulate diverse aspects of the APAP-induced injury response; regulation of cell death (*Bax*) and metabolism (*Sdhb*), recruitment (*Ccl4*, *Ccl5*, *Ccr2*) and cell adhesion (*Icam1*, *Itgam*), as well as immune activation (*Ltb*, *Tgfb1*) and breakdown of reactive oxygen species (*Sod1*, *Sod2*). *Mmp13* from activated KCs was predicted to impact gene expression in 22 cell types via *Cd11b* and/or *Lrp1* and was implicated largely in the regulation of targets involving cell death and proliferation (*Cdkn1a*, *Ubc*, *Bcl9l*, *Bcl2l1*, *Ets1*, *Ptma*) and cell structure maintenance (*Ahnak*, *Lmna*, *Plec*) (Figure S2E). Of the top regulators identified by NicheNet, *Il12b* from activated cDC1s had the highest average regulatory potential among the downstream target genes. *IL12b* was identified as upstream of putative interactions involving 13 cell types via activity in the form of either IL-12 and IL-23 through *Il23r*, *Il12rb1*, or *Il12rb2*. Analysis of downstream targets suggested that activated cDC1s regulate various functions post-APAP treatment involving lymphocyte recruitment (*Ccl4*, *Cd3e*, *Cxcl9*) and activation (*Il1b*, *Irf1*, *Fos*), as well as mitigation of DNA-damage associated responses (*Gadd45g*) (Figure 2F). Together, these data suggest that tissue-resident KCs and cDC1s, in addition to recruited LAMs, largely coordinate the immediate response to sterile liver injury *in silico*.

Hematopoietic IL-12 signaling protects against acute liver injury

Although our NicheNet analysis identified *IL12b* as a putative upstream regulator of the transcriptional response to sterile liver injury, the role of IL-12 signaling during drug-induced acute liver injury is unclear.[22,23] To investigate whether IL-12b plays a role during acute liver injury, we intraperitoneally injected APAP into IL-12b-deficient (*IL12b*$^{-/-}$) or WT mice to induce acute liver injury and then analyzed alanine aminotransferase (ALT) concentrations in the plasma 24, 48, and 72 h later. *IL-12b*$^{-/-}$ mice had significantly increased plasma ALT levels 24 and 48 h post-injection compared with WT mice (Figure 3A), suggesting that IL-12 may play a protective role during drug-induced acute liver injury in mice. To confirm this hypothesis, we utilized another mouse model of acute liver injury using carbon tetrachloride (CCl_4).[24] *IL-12b*$^{-/-}$ or WT mice were intraperitoneally injected with CCl_4, and plasma ALT concentrations were measured 48 h later. Consistent with our previous results, CCl_4-treated *IL-12b*$^{-/-}$ mice had significantly increased plasma ALT levels compared with WT controls (Figure 3B). Moreover, we found that CCl_4-treated *IL-12b*$^{-/-}$ mice had increased centrilobular hepatocyte necrosis, indicating greater damage around the central veins in the liver compared with CCl_4-treated WT mice (Figures 3C and 3D). Finally, treatment of WT mice with a neutralizing monoclonal antibody (mAb)

against IL-12b significantly increased ALT concentrations after CCl_4 injection compared with isotype-matched immunoglobulin (Ig)-treated mice (Figure 3E). Because IL-12b is a common subunit of both IL-12 and IL-23,[25] we were unable to attribute these protective effects to a specific cytokine signaling pathway. To resolve this, we generated bone marrow chimeric mice utilizing WT hosts reconstituted with either WT, IL-12 receptor-deficient (*Il12rb2*$^{-/-}$), or STAT4-deficient (*Stat4*$^{-/-}$) bone marrow to generate bone marrow chimeric mice with hematopoietic-derived cells deficient in IL-12 signaling.[25,26] Both *IL12rb2*$^{-/-}$ and *STAT4*$^{-/-}$ recipient mice had significantly increased plasma ALT levels compared with WT recipient mice 48 h following CCl_4 treatment (Figure 3F), suggesting that IL-12 signaling in hematopoietic-derived cells is protective during acute sterile liver injury in mice.

cDC1-derived IL-12 protects against acute sterile liver injury

Because our scRNA-seq dataset identified activated cDC1s as the cellular source of *I12b* during liver injury, we utilized *Il12b*$^{tm1.1Lky/J}$ (*Il12b*^{YFP}) reporter mice[27] to confirm this *in silico* finding. Unbiased analysis of total YFP^+ cells revealed a 7-fold induction of YFP^+ cells 24 h post-CCl_4 treatment. Furthermore, more than 70% of IL-12-producing cells could be identified as $CD45^+Lin^-CD88^-MHCII^+CD11c^+CD11b^-XCR1^+$ cells, consistent with the canonical description of cDC1s[28] (Figure S3A). We did not observe significant $CD45^+Lin^-CD88^+YFP^+$ macrophage or $CD45^+Lin^-CD88^-MHCII^+CD11c^+CD11b^+XCR1^-YFP^+$ cDC2 populations at any time points post-CCl_4 treatment (Figures 4A, 4B, and S1D), confirming our scRNA-seq analysis that cDC1s are the major early producers of IL-12 after acute sterile liver injury. This result was not limited to CCl_4-induced injury, as APAP treatment also induced robust IL-12 signals from cDC1, but not cDC2 or macrophage, populations from *Il12-b*^{YFP} mice 24 h post-injection (Figure S3B).

To determine whether cDC1s contributed to protective responses during acute sterile liver injury, we used *Xcr1*^{DTR} mice, which allow for diphtheria toxin (DT)-mediated specific inducible depletion of cDC1s.[29] Whereas DT treatment completely ablated liver cDC1s, adoptive transfer of bone marrow-derived cDC precursors (cDCPs), which develop into mature cDC1s *in vivo*, rescued both the frequencies and numbers of cDC1s in the liver[30] (Figures 4C–4F). DT treatment only ablated cDC1 populations, as liver cDC2 frequencies and numbers were unaffected (Figures S3C and S3D). To test whether cDC1s are required for protection during acute injury, *Xcr1*^{DTR} mice were treated with PBS or DT followed by CCl_4 24 h later. Analysis of plasma ALT concentrations 48 h post-CCl_4 treatment showed a significant increase in ALT levels in DT-treated *Xcr1*^{DTR} mice compared with PBS controls (Figure 4G). This affect was not due to off-target effects of DT, as DT treatment of WT mice did not affect ALT levels post-CCl_4 (Figure S3E). Furthermore, adoptive transfer of 1×10^7 WT cDCPs or *IL-12b*$^{-/-}$ cDCPs into DT-treated *Xcr1*^{DTR} mice 1 day prior to CCl_4 treatment significantly reduced and increased ALT levels, respectively (Figure 4G), indicating that cDC1-derived IL-12 protected against sterile liver injury.

cDC1-derived IL-12 is required for liver ILC1 IFN-γ production following acute injury

IFN-γ produced by liver-resident ILC1s has been recently implicated in protective responses during acute liver injury via upregulation of Bcl-xL in hepatocytes.[31] As

IL-12 signaling can drive tissue-resident ILC1 IFN-γ production during inflammation in other peripheral tissues,[32–35] we hypothesized that cDC1s could facilitate protective effects during acute liver injury via activation of liver-resident ILC1s. We therefore investigated whether cDC1s were required for optimal production of IFN-γ by ILC1s. *Xcr1*^{DTR} mice were treated with DT or PBS and then injected with CCl_4 before livers were harvested and processed 18 h later. Of the liver group 1 ILCs analyzed, IL-18r$^+$ ILC1 (CD45$^+$Lin$^-$NK1.1$^+$CD200r$^+$CD49b$^-$IL18r$^+$) produced the most IFN-γ, while neither IL-18r$^-$ cytotoxic ILC1s (CD45$^+$Lin$^-$NK1.1$^+$CD200r$^+$ CD49b$^-$IL18r$^-$)[36] nor NK cells (CD45$^+$Lin$^-$NK1.1$^+$CD200r$^-$CD49b$^+$) displayed robust IFN-γ production in response to CCl_4 treatment (Figures 5A, 5B, and S4A). Importantly, IFN-γ production was reduced in all group 1 ILCs upon DT-mediated depletion of cDC1 and could be restored upon adoptive transfer of WT cDCPs into DT-treated *Xcr1*^{DTR} mice (Figures 5A and 5B). Adoptive transfer of WT cDCPs similarly restored the number of IFN-γ-producing cells in all group 1 ILC populations in the liver following CCl_4 injection (Figures 5C and 5D). These observations are consistent with previous work highlighting increased IFN-γ production from activated CD25$^+$ ILC1 subsets but not from CD25$^-$ ILC1 or NK cells[31] (Figure S4B). However, we found that CD25 expression on ILC1 and CD25$^+$ ILC1 numbers, but not IL18r expression nor IL18r$^+$ ILC1 numbers, were dependent on liver cDC1s (Figures S4C–S4F). These results suggested that CD25 expression on liver ILC1s likely reflects an activation state. Notably, IL18r$^+$ ILC1 numbers were decreased after CCl_4 treatment in all cohorts (Figure S4F), consistent with previous reports that this population is reduced during inflammation.[37] Critically, group 1 ILC IFN-γ production was reduced in *Xcr1*^{DTR} mice that were adoptively transferred with *IL12b*$^{-/-}$ cDCPs (Figures 5A–5D), suggesting that cDC1-derived IL-12 was required for optimal IFN-γ responses during liver injury.

To confirm that IL-12 signaling was critical for ILC1 IFN-γ production, we analyzed liver group 1 ILC subsets from mixed bone marrow chimeric mice utilizing congenically distinct WT (CD45.1) hosts reconstituted with either *IL12rb2*$^{-/-}$ or *STAT4*$^{-/-}$ (CD45.2) bone marrow and then treated each cohort with CCl_4. Our results suggested that IL-12 signaling was indeed necessary for optimal IFN-γ responses 18 h post-CCl_4 treatment, as IL-18r$^+$ ILC1 IFN-γ production was greatly reduced in knockout (KO) cells compared with WT cells from WT:I*L12rb2*$^{-/-}$ and WT:*STAT4*$^{-/-}$ mice (Figure 5E). IFN-γ production was comparably reduced in NK cells derived from the KO bone marrow in WT:*IL12rb2*$^{-/-}$ and WT:*STAT4*$^{-/-}$ mice (Figure 5F). Together, these results demonstrate that cDC1-derived IL-12 is required for group 1 ILC IFN-γ production during acute liver injury.

cGAS-STING signaling is required for cDC1-derived IL-12 production during liver injury

IL-12 is induced via activation of the noncanonical nuclear factor κB (NF-κB) pathway in response to various upstream mechanisms, including tumor necrosis factor receptor superfamily member signaling.[38,39] However, numerous innate immune sensing pathways have the capacity to activate NF-κB signaling in response to both pathogen-associated and damage-associated molecular patterns.[40] As a central regulator of immune function, we sought to identify the potential mechanism(s) by which NF-κB and, subsequently, cDC1 and IL-12 responses become activated during acute liver injury. We first optimized an adoptive transfer system whereby 1×10^7 *Il12b*^{YFP} bone marrow-derived cDCPs could

be adoptively transferred into DT-treated *Xcr1*^{DTR} hosts before initiation of acute liver injury using CCl_4 (Figure 6A). In this model, CCl_4, but not vehicle treatment, induced robust IL-12 responses from adoptively transferred cDC1s isolated from the liver 24 h later (Figures 6B and 6C). We then paired our adoptive transfer model with a CRISPR-Cas9 ribonucleoprotein (cRNP) genomic editing approach[30,41] to genetically delete components of the Toll-like receptor, retinoic acid inducible gene I (RIG-I) like receptor, inflammasome, or cytosolic DNA-sensing pathways from cDCPs prior to adoptive transfer (Figure 6A). High-efficiency KO gRNAs were identified for target genes: *Myd88*, *Mavs*, *Nlrp3*, *Aim2*, *Mb21d1* (cGAS), and *Tmem173* (STING). Efficient KOs were validated via immunoblot (Figures S5A and S6A–S6C). *In vivo*, only *Tmem173* cRNP-edited cDC1s had significantly reduced IL-12 production compared with nontargeting control (NTC) cRNP-edited cDC1s after CCl_4 treatment (Figure 6D), suggesting a potential role for nucleic acid sensing in cDC1 activation during liver injury. While neither *Myd88* nor *Nlrp3* cRNP-edited cDC1s displayed different frequencies of YFP^+ cells following adoptive transfer, both *Mavs* and *Aim2* cRNP-edited cDC1s displayed increased YFP^+ frequencies compared with NTC cRNP-edited cDC1s (Figure 6D). These results indicated that while *Mavs* and *Aim2* may negatively regulate cDC1 IL-12 production during liver injury, cDC1-intrinsic STING signaling was required for IL-12 production. To confirm the importance of STING in cDC1 IL-12 production, we utilized a separate mouse model where we treated *Il12b*^{YFP} or *Il12b*^{YFP} × *Tmem173*^{Gt} STING-deficient mice (hereafter referred to as *Il12b*^{YFP} × Sting^{Gt}) with CCl_4 and then assessed liver cDC1 IL-12 production 24 h later. Indeed, *Il12b*^{YFP} × Sting^{Gt} mice had significantly reduced cDC1 IL-12 production compared with STING-sufficient controls (Figure 6E). Moreover, adoptive transfer of *Il12b*^{YFP} × Sting^{Gt} cDCPs into DT-treated *Xcr1*^{DTR} hosts resulted in reduced IL-12 from STING-deficient cDC1s compared with WT controls after CCl_4 treatment (Figure 6F). Together, these results suggest a previously unknown role for cytosolic DNA sensing in liver cDC1s through cGAS-STING signaling to induce protective sterile inflammation during liver injury.

Cytosolic DNA binding by cGAS catalyzes the production of the second messenger 2′3′-cyclic GMP-AMP (cGAMP), which binds and activates endoplasmic reticulum-associated STING leading to NF-κB and MAPK signaling downstream.[42] However, secreted 2′3′-cGAMP is capable of bypassing cytosolic DNA sensing by cGAS and activating STING in neighboring cells in a paracrine manner.[43–46] As such, cGAS activation in other cell types may indirectly contribute to activation of STING signaling within cDC1s during sterile liver injury. To test whether or not exogenous sources of 2′3′-cGAMP from structural cell cGAS activation contribute to IL-12 production in cDC1, we utilized a bone marrow chimeric approach where either WT or *cGAS*$^{-/-}$ hosts were reconstituted with *Il12b*^{YFP} bone marrow. Both cohorts of mice were treated with CCl_4, and liver cDC1 IL-12 production was assessed 24 h later. No differences were observed between groups (Figure 6G), suggesting that parenchymal cGAS signaling did not contribute to cDC1 IL-12 production. In agreement with this finding, analysis of bone marrow chimeric mice revealed that only hematopoietic-derived cGAS deficiency was required for liver injury protection, as both *cGAS*$^{-/-}$ (host):*cGAS*$^{-/-}$ (bone marrow [BM]) and WT (host):*cGAS*$^{-/-}$ (BM), but not *cGAS*$^{-/-}$ (host):WT (BM) nor WT (host):WT (BM), bone marrow chimeric mice had increased plasma ALT levels after CCl_4 treatment (Figure 6H). To confirm the importance of

cDC1 intrinsic cGAS signaling, we again used our cRNP adoptive transfer method to ablate cGAS in adoptively transferred cDCPs before initiation of acute injury. Similar to *Tmem173* cRNP-edited cDC1s, *Mb21d1* cRNP-edited cDC1s had reduced IL-12 levels compared with NTC cRNP-edited cDC1s (Figure 6I). Together, these data indicate that cDC1-derived IL-12 mediates protection during acute sterile liver injury via intrinsic activation of the cGAS-STING pathway.

DISCUSSION

In this study, we analyzed liver scRNA-seq datasets from WT and APAP-treated mice to identify *Il12b* from activated cDC1 as a putative regulator of acute liver injury-induced changes in gene expression. Using *in vivo* mouse models, we confirmed that IL-12 signaling was protective during drug-induced acute liver injury. *Il12b*-deficient mice had increased plasma ALT levels and centrilobular hepatocyte necrosis compared with WT controls. Furthermore, inducible depletion of IL-12-producing $XCR1^+$ cDC1s increased liver injury and reduced liver-resident ILC1 IFN-γ production. Adoptive transfer of cDC1s reduced plasma ALT levels and increased ILC1 IFN-γ production in cDC1-deficient mice, suggesting that cDC1s induce an early protective tissue-resident immune response during sterile liver injury. Using a targeted CRISPR screen of innate immune sensing pathways and KO mice, we found that cDC1-intrinsic cGAS-STING signaling was required for cDC1 IL-12 production. Altogether, our data suggest that cDC1s protect against sterile injury via cell-intrinsic activation of cGAS-STING and production of IL-12.

Using *in silico* single-cell receptor-ligand analysis, we identified putative upstream transcriptional regulators produced by tissue-resident innate immune populations enriched during acute liver injury. LAMs were identified as major producers of *Ccl2*, *Ccl12*, and *Ccl7*, highlighting their importance in mediating recruitment of other immune cell types into the liver microenvironment during injury. Consistent with previous reports, these cells likely orchestrate critical early innate and adaptive immune cell activation to mitigate damage and to promote inflammation and tissue remodeling.[15,47,48] During liver injury, metalloproteases have been shown to be critical regulators of fibrosis regression and recovery.[49,50] Our analysis suggested that *Mmp13* expressed by activated KCs may be involved in regulating cell death progression and cell structural maintenance, especially in nonimmune cells. Indeed, *Mmp13* has been shown to play a critical role in the resolution of hepatic fibrosis,[51] supporting our findings that activated KCs may contribute to the early immune-parenchymal cell responses during acute injury. Finally, our analysis identified *Il12b* from activated cDC1s as having the highest average regulatory potential among the top 20 key regulators, many of which have previously been implicated in the response to liver injury: *Icam1*,[52,53] *Il1a*,[54] *Il18*,[55,56] *Mmp13*,[51] *Ccl2*,[17] *Hbegf*,[57] and *Cd40*.[58] As *Il12b* was uniquely expressed by activated cDC1s, these results suggested a critical contribution of IL-12b and cDC1s to injury-induced changes in gene expression.

Previous studies have suggested that DCs contribute to fibrosis resolution and prevention of NASH-associated inflammation.[59,60] However, use of transgenic mouse models utilizing CD11c-driven ablation is not able to define the precise contribution of DCs, as CD11c can be expressed by monocyte and monocyte-derived macrophage subsets, which have also been

suggested to play protective roles during liver injury.[15,17,47,48] More recent work utilizing *Batf3*-deficient mouse models suggested that DCs limit NASH development,[61] but *Batf3* can also be expressed by other cell types *in vivo* including CCR6$^+$ ILC3s,[62] while also impacting CD8$^+$ T cell memory and Treg development in the periphery.[63,64] In contrast to these previous findings, a recent study utilizing cDC1-specific KO mice found that cDC1s can drive liver pathology during NASH,[65] consistent with another earlier report suggesting that DCs contribute to inflammation and liver fibrosis.[66] While our study suggests that cDC1s are protective during acute liver injury, IL-12 from cDC1s or IFN-γ from ILC1s may play beneficial roles during acute inflammation but may become detrimental at increased concentrations or during periods of long-term chronic activation.[67–69] Because DCs have been shown to regulate burn wound healing by enhancing early endothelial cell proliferation and vascularization,[70] DC tissue protective function is likely not limited to the liver following acute injury. Thus, while tissue-resident cDC1s may serve differential roles in acute versus chronic inflammation, the cDC1 response to acute tissue injury may be largely protective in peripheral tissues.

Our study also identified a key role for cGAS-STING signaling in IL-12 production by cDC1s during acute liver injury. Because non-hematopoietic cell-derived cGAS signaling was not required for IL-12 production by cDC1s, our results suggest that STING signaling in liver cDC1s is not due to uptake of extracellular 2′3′-cGAMP. Instead, our results suggest that this process requires cytosolic DNA sensing by cDC1s. While recognition of self-, cell-free DNA by cGAS is typically associated with autoimmunity,[42,71] uptake of tumor-derived DNA by DCs and subsequent activation of cGAS-STING signaling has been shown to promote beneficial anti-tumor responses.[72–74] Our results suggest that a similar mechanism may occur during acute liver injury, supporting previous studies that associate dead and dying hepatocyte DNA sensing with liver inflammation during APAP overdose.[75–77] In this context, uptake of dead or dying hepatocyte-derived DNA by cDC1 and cGAS-STING activation may drive protective IL-12 responses. However, it is still unclear whether cDC1s take up cell-free DNA during acute liver injury and how extracellular DNA might escape degradation within the phagolysosome after uptake. Future research will be required to determine whether there are direct mechanisms that mediate extracellular DNA uptake by cDC1s during liver injury.

In summary, our study utilized single-cell network analyses and comprehensive *in vivo* models to validate a previously unclear mediator of acute injury-associated sterile inflammation. Our work demonstrates the power of unbiased cell-cell interaction analytical techniques to identify key regulatory cell types and signals within publicly available scRNA-seq datasets. We discovered the mechanisms by which cDC1-derived IL-12 contributes to protective inflammatory responses during acute liver injury. Finally, we uncovered the pathway by which cDC1s initiate acute sterile inflammation, implicating these cells as protective tissue-resident sentinels of tissue injury.

Limitations of the study

Our study focused on the early activated cell types during acute liver injury to drive protective sterile inflammatory responses. Although scRNA-seq and receptor-ligand analysis

enabled the identification of key regulators of injury-induced transcriptional changes, it should be noted that the analyzed scRNA-seq dataset was unable to completely resolve the full extent of previously reported liver macrophage heterogeneity. The absence of some of these populations within this scRNA-seq dataset meant that we were unable to assess the putative interactions that occur involving these cells during acute liver injury. Future datasets with increased cells sequenced or sequencing depth will be required to determine the putative signals to and from these populations and how they may regulate early sterile inflammation. In addition, our results suggest that cDC1-derived IL-12 is required for optimal IFN-γ production by group 1 ILCs during acute liver injury. However, adoptive transfer of *IL12b*$^{-/-}$ cDCPs did not completely abrogate IFN-γ production to similar levels as those present in cDC1-deficient mice. Thus, there are likely additional cDC1-intrinsic or -extrinsic mechanisms that contribute to IFN-γ production by NK cells and ILC1s during acute liver injury.

STAR★METHODS

RESOURCE AVAILABILITY

Lead contact—Further information and requests for resources, reagents or materials should be directed to, and will be fulfilled by the lead contact, Timothy O'Sullivan (tosullivan@mednet.ucla.edu).

Materials availability—This study did not generate new unique reagents.

Data and code availability

- This paper analyzes existing, publicly available data. These accession numbers for the datasets are listed in the key resources table. All original sequencing data have been deposited at Zenodo repository and are publicly available under the following URL: https://doi.org/10.5281/zenodo.6035873. DOI is also listed in the key resources table.
- This paper does not report original code. All codes used in this paper are available from the lead contact upon request.
- Any additional information required to reanalyze the data reported in this paper is available from the lead contact upon request.

EXPERIMENTAL MODEL AND SUBJECT DETAILS

Mice—Mice were bred at UCLA in accordance with the guidelines of the institutional Animal Care and Use Committee (IACUC). The following mouse strains were used this study: C57BL/6 (CD45.2) (Jackson Labs, #000664), B6.SJL (CD45.1) (Jackson Labs, #002114), B6(C)-*Cgas*$^{tm1d(EUCOMM)Hmgu}$/J (cGAS$^{-/-}$) (Jackson Labs, #026554), B6.129S1-*Il12b*^{tm1Jm}/J (*Il12b*$^{-/-}$) (Jackson Labs, #002693), *B6.129-Il12b*$^{tm1.1Lky}$*/J* C57BL/6J-*Sting1*^{gt}/J (*Il12b*^{YFP}×Sting^{Gt}), *Xcr1*$^{+/DTRvenus}$,[29] *Il12b*$^{tm1.1Lky}$*/J* (*Il12b*^{YFP}) (Jackson Labs, #006412), *Tmem173*^{gt} (Sting^{Gt}) (Jackson Labs, #017537), *B6;129S1-Il12rb2*^{tm1Jm}*/J* (*Il12rb2*$^{-/-}$) (Jackson Labs, #003248), and *C57BL/6J-Stat4*^{em3Adiuj}*/J* (*Stat4*$^{-/-}$) (Jackson

Labs, #028526). Experiments were conducted using 6–10-week-old age-and gender-matched mice in accordance with approved institutional protocols.

APAP-induced liver injury—Mice were fasted for 12 hours with free access to water prior to treatment. 15 mg/mL APAP (Sigma-Aldrich) was freshly prepared in 1X PBS and placed at 37°C until completely dissolved. Mice were intraperitoneally injected with 300 mg/kg body weight of APAP, and had free access to food, water, bedding, and feces after APAP injection. Blood was collected 24, 48, and 72 hours after APAP injection and plasma samples were prepared by centrifugation at 500 × g for 20 min at 4°C. Concentrations of ALT in the plasma were measured by using the Pointe Scientific ALT (SGPT) Liquid Reagents (Fisher Scientific) and analyzed using a Synergy 2 microplate reader (BioTek).

CCl_4-induced liver injury—Mice were intraperitoneally injected with 10μL 10% CCl_4 (Sigma-Aldrich) in corn oil (Sigma-Aldrich) per gram body weight. Blood was collected 48 hours after CCl_4 injection and plasma samples were prepared by centrifugation at 500 × g for 20 min at 4°C. Concentrations of ALT in the plasma were measured by using the Pointe Scientific ALT (SGPT) Liquid Reagents (Fisher Scientific) and analyzed using a Synergy 2 microplate reader (BioTek). To block cytokine signaling, mice were intraperitoneally injected with 250μg neutralizing mAb against mouse IL-12p40 (clone C17.8, Bio X Cell) or isotype-matched immunoglobulin rat IgG2a (clone 2A3, Bio X Cell) 12 hours before and after CCl_4 injection.

Bone marrow-derived cDCP culture—To generate bone marrow derived cDCPs, bone marrow leukocytes were resuspended at 1.5×10^7 cells/10mL in DC media (RMPI 1640 + 25mM HEPES +10% FBS, 1% L-glutamine, 1% 200mM sodium pyruvate, 1% MEM-NEAA, 1% penicillin-streptomycin, 0.5% sodium bicarbonate, 0.01% 55 mM 2-mercaptoethanol supplemented with 200 ng/mL FLT3-L and 5 ng/mL GM-CSF) and then plated in 10cm non-TC treated culture dishes (Corning) and incubated at 37°C. BMDC1 were cultured for 9 days in DC media with an additional 5 mL of DC media added on Day 5. Cells were either harvested on Day 9 for cRNP editing and/or adoptive transfer, or media was changed and bone marrow cDC1 were used for experiments on D15.[30,81]

METHOD DETAILS

Cell clustering and cell-type annotation—The R package Seurat (v.3.1.2),[79] was used to cluster the cells in the merged matrix. Cells with <200 transcripts detected or >5% mitochondrial gene expression were first filtered out as low-quality cells. The gene counts for each cell were divided by the total gene counts for the cell and multiplied by a scale factor of 10,000, then natural-log transformation was applied to the counts. The FindVariableFeatures function was used to select variable genes with default parameters. The ScaleData function was used to scale and center the counts in the dataset. Principal component analysis was performed on the variable genes, and 30 principal components were used for cell clustering (resolution = 0.5) and UMAP dimensional reduction. The cluster markers were found using the FindAllMarkers function, and cell types were manually annotated based on the cluster markers. To calculate the sample composition based on cell type, the number of cells for each cell type from each sample were counted. The counts

were then divided by the total number of cells for each sample and scaled to 100% for each cell type. Subclustering was performed on all cell types. The same functions described above were used to obtain the subclusters. Subclusters that were defined exclusively by mitochondrial gene expression, indicating low quality, were removed from further analysis.

CellChat analysis—The R package CellChat was utilized to identify and visualize cell-cell interactions between Healthy and APAP-treated mice. The standard preprocessing steps were applied to the loaded the normalized counts, including the functions identifyOverExpressedGene and identifyOverExpressedInteractions using a standard parameter set. Only interactions from "secreted signaling" databases were utilized for cell-cell communication analysis. Cell-cell communications with fewer than 10 cells in cell groups were filtered out. We then calculated the potential ligand-receptor interactions between cells from WT and APAP-treated mice based on the functions computeCommunProb, computeCommunProbPathway, and aggregateNet using standard parameters. Alluvial plots were utilized to show the associations of latent patterns of signaling pathways. Incoming and outgoing cell patterns and communication patterns of secreting cells were determined utilizing the R package NMF. The selectK function was utilized to infer the number of patterns based on similarities of ligand-receptor pairs and cell groups as measured by Cophenetic and Silhouette values.

NicheNet analysis—The R package NicheNet was utilized to predict the potential ligand–receptor communication between Healthy and APAP-treated mice. Briefly, cell types differentially enriched in APAP-treated mice were defined as sender cell populations, including cDC1, Activated cDC1, KC, Activated KC, Monocytes, and LAMs. The gene set of interest analyzed consisted of genes that NicheNet's algorithm identified as being differentially expressed after APAP-treatment based on the standard Seurat Wilcoxon test. The top 20 ranked ligands were utilized for downstream analyses of regulatory potential. To visualize ligand-target and ligand-receptor interactions, only ligands unique to APAP-enriched cell states were utilized. Ligand-target links belonging to the lowest 60% of scores were removed. Ligand-receptor links belonging to the lowest 40% of scores were removed.

Isolation of mouse lymphocytes and dendritic cells—Mouse livers and bone marrow were harvested and prepared into single cell suspensions.[35] Briefly, to isolate liver lymphocytes, the tissues were physically dissociated using a glass tissue dounce homogenizer and purified using of 40% Percoll (VWR). After centrifugation at 2000rpm for 5 minutes at room temperature, the pellets were resuspended in 1X PBS and filtered using 100μm strainers. To harvest bone marrow, the tibia, fibula, and femur were removed and then crushed using mortar and pestle in 1X PBS. The resulting mixture was filtered using 100μm strainers and centrifuged. Red blood cells in the liver and bone marrow were lysed using ACK lysis buffer. The resulting pellets were either plated for bone marrow cDCP generation or analyzed via flow cytometry.

Isolation of liver macrophage subsets—Mouse livers were harvested and prepared into single cell suspensions,[82] with some modifications. Livers were initially perfused with 1X PBS before removal of the left lateral lobe and dissociation using a razor blade in 8mL

digestion buffer (DMEM + 10%FBS + 0.75mg/mL Collagenase A (Roche) + 50 μg/mL DNase 1 (Roche) on ice. After warming to 37°C for 5 minutes, samples were placed in a 37°C shaking incubator (225rpm) to digest for 30 minutes, vortexing samples after 15 minutes. Samples were then filtered using a 70μm cell strainer and 10mL cold DMEM +10%FBS was added to inactivate enzymatic activity. Remaining undigested liver pieces were mashed using the end of a syringe plunger before addition of another 5mL cold DMEM +10%FBS to wash. Samples were then centrifuged at 50 × g for 3 minutes at 4°C with low acceleration and deceleration. The resulting supernatant, containing the hepatic macrophages, was removed and then centrifuged again at 200 × g for 7 minutes at 4°C with low acceleration and deceleration before lysis of red blood cells using ACK lysis buffer. The resulting pellets were analyzed by flow cytometry.

CRISPR-Cas9 ribonucleoprotein (cRNP) genomic editing—Guide RNA design, cRNP complex formation, and electroporation were performed.[30,41] Guide RNA sequences were derived from recent whole-genome-based CRISPR-Cas9 KO libraries[78] and ordered from SYNTHEGO. 1×10^6 D9 cDCPs in T Buffer (ThermoFisher) per reaction were combined complexed cRNP and then electroporated using the Neon Transfection system (ThermoFisher) at pulse code 1900V 20ms × 1 pulse. Immediately following electroporation, cells were either centrifuged, resuspended in 1× PBS and then adoptively transferred or resuspended in DC media to dilute T buffer and incubated at 37°C for 90 minutes. Cells were then centrifuged and resuspended in DC media before culturing *in vitro*. Cells were cultured *in vitro* for 6 days following electroporation prior to reading out gene editing efficiency by sanger sequencing or isolation of protein for immunoblot analysis.

Diphtheria toxin treatment and depletion of XCR1-expressing cells—Diphtheria toxin (DT), unnicked (List Biological Laboratories), was injected intraperitoneally at a dose of 4 ng/g body weight in 1X PBS. 1X PBS alone was used as a control. DT dose was determined based on the efficiency of deletion of XCR1-expressing cells at titrated doses.

Adoptive transfer experiments—1×10^7 cDCPs were transferred i.v. into recipient DT-treated $Xcr1^{DTR}$ hosts 1 day before CCl_4 treatment. In other experiments, cDCPs were electroporated using the conditions described above before transfer i.v. into recipient DT-treated $Xcr1^{DTR}$ hosts 1 day before CCl_4 treatment.

***Ex vivo* culture of lymphocytes—**Isolated liver lymphocytes were stimulated for 5 hours in CR-10 media (RMPI 1640 + 25mM HEPES +10% FBS, 1% L-glutamine, 1% 200mM sodium pyruvate, 1% MEM-NEAA, 1% penicillin-streptomycin, 0.5% sodium bicarbonate, 0.01% 55 mM 2-mercaptoethanol) containing Brefeldin A (1:1000; BioLegend) and Monensin (2uM; BioLegend) prior to analysis of IFN-γ production. Cells were cultured in media alone as a negative control.

Flow cytometry—Cells were analyzed for cell-surface markers using fluorophore-conjugated antibodies (BioLegend, eBioscience). Cell surface staining was performed in 1X PBS and intracellular staining was performed using the eBioscience Foxp3/Transcription Factor kit. Flow cytometry was performed using the Attune NxT and data were analyzed with FlowJo software (BD). Cell surface and intracellular staining was performed using

the following fluorophore-conjugated antibodies: CD45.1 (A20), CD45.2 (104), NK1.1 (PK136), CD49b (DX5), TCRβ (H57–597), CD3 (17A2), CD200r1 (OX-110), CD25 (PC61), IL-18r (P3TUNYA), IFN-γ (XMG1.2), I-A/I-E (M5/114.15.2), CD19 (6D5), CD11c (N418), CD11b (M1/70), XCR1 (Zet), Ly6G (1A8), CD88 (20/70), F4/80 (BM8), Tim-4 (RMT4–54), Ly6C (HK1.4), CX3CR1 (SA011F11), and CD9 (MZ3).

Histology—Left lateral lobes from livers of naive and CCl_4-injected mice were resected and then fixed with formalin and embedded in paraffin 48 hours after injection. Fixed histological sections were stained with hematoxylin and eosin. Images were acquired using a Keyence BZ-X710 microscope, and centrilobular hepatocyte necrosis and damaged area around the central veins was quantified using QuPath.[80]

Immunoblot—Protein was extracted from D15 cRNP-edited bonne marrow cDC1 using Pierce RIPA buffer (Thermo-Fisher) with Halt protease inhibitor cocktail (Thermo-Fisher) and protein concentration was quantified using the Pierce BCA Protein Assay kit (Thermo-Fisher). Samples were electrophoresed on NuPage Novex 4–12% Bis-Tris Protein Gels, transferred to PVDF membranes, and blocked for one hour at room temperature with 5% w/v nonfat milk in 1X TBS and 0.1% Tween-20. Immunoblots were performed using rabbit anti-STING (D2P2F) (Cell Signaling), rabbit anti-AIM2 (Mouse Specific) (Cell Signaling), rabbit anti-NLRP3 (D4D8T) (Cell Signaling), rabbit anti-MAVS (Rodent Specific) (Cell Signaling), rabbit anti-MyD88 (D80F5) (Cell Signaling), rabbit anti-cGAS (D3O8O) (Cell Signaling), and rabbit anti-β-actin (Cell Signaling CST4970). Proteins were detected using the SuperSignal West Pico PLUS ECL kit (Thermo-Fisher) and visualized using the Azure Biosystems c280 imager.

PCR and sanger sequencing—DNA from cRNP-edited bone marrow cDC1 was isolated using DNeasy Blood and Tissue kits (Qiagen). DNA concentration was measured using the NanoDrop OneC Microvolume UV-Vis Spectrophotometer (ThermoScientific) and then diluted to 50 ng/μL in water before PCR amplification of cRNP-targeted genomic regions (Table S8). PCR samples from NTC and Target cRNP-edited cells were submitted for sanger sequencing (GENEWIZ) and then indel percentage was calculated using ICE analysis (SYNTHEGO).

QUANTIFICATION AND STATISTICAL ANALYSIS

For graphs, data are shown as mean ± s.e.m. and, unless otherwise indicated, statistical differences were evaluated using a Student's t test with Welch's correction to assume a non-normal variance in our data distribution. $p < 0.05$ was considered significant. Graphs were produced and statistical analyses were performed using GraphPad Prism.

Supplementary Material

Refer to Web version on PubMed Central for supplementary material.

ACKNOWLEDGMENTS

We thank members of the O'Sullivan, Su, Covarrubias, and Seki labs for helpful discussions. A.D.H was supported by the NIH National Research Service Award F31, NIDDK (F31DK130585). T.E.O. was supported by the NIH (AI145997).

INCLUSION AND DIVERSITY

We worked to ensure sex balance in the selection of nonhuman subjects. One or more of the authors of this paper self-identifies as an underrepresented ethnic minority in their field of research or within their geographical location. One or more of the authors of this paper received support from a program designed to increase minority representation in their field of research. While citing references scientifically relevant for this work, we also actively worked to promote gender balance in our reference list. We avoided "helicopter science" practices by including the participating local contributors from the region where we conducted the research as authors on the paper. We support inclusive, diverse, and equitable conduct of research.

REFERENCES

1. Meizlish ML, Franklin RA, Zhou X, and Medzhitov R (2021). Tissue homeostasis and inflammation. Annu. Rev. Immunol 39, 557–581. 10.1146/annurev-immunol-061020-053734. [PubMed: 33651964]
2. Chen GY, and Nuñez G (2010). Sterile inflammation: sensing and reacting to damage. Nat. Rev. Immunol 10, 826–837. 10.1038/nri2873. [PubMed: 21088683]
3. Grivennikov SI, Greten FR, and Karin M (2010). Immunity, inflammation, and cancer. Cell 140, 883–899. 10.1016/j.cell.2010.01.025. [PubMed: 20303878]
4. Kubes P, and Mehal WZ (2012). Sterile inflammation in the liver. Gastroenterology 143, 1158–1172. 10.1053/j.gastro.2012.09.008. [PubMed: 22982943]
5. Huber-Lang M, Lambris JD, and Ward PA (2018). Innate immune responses to trauma. Nat. Immunol 19, 327–341. 10.1038/s41590-018-0064-8. [PubMed: 29507356]
6. Kulkarni OP, Lichtnekert J, Anders H-J, and Mulay SR (2016). The immune system in tissue environments regaining homeostasis after injury: is "inflammation" always inflammation? Mediat. Inflamm. 2016, 2856213–2856219. 10.1155/2016/2856213.
7. Yoon E, Babar A, Choudhary M, Kutner M, and Pyrsopoulos N (2016). Acetaminophen-induced hepatotoxicity: a comprehensive update. J. Clin. Transl. Hepatol 4, 131–142. 10.14218/JCTH.2015.00052. [PubMed: 27350943]
8. Jaeschke H, and Ramachandran A (2020). Mechanisms and pathophysiological significance of sterile inflammation during acetaminophen hepatotoxicity. Food Chem. Toxicol 138, 111240. 10.1016/j.fct.2020.111240. [PubMed: 32145352]
9. Andrews TS, Atif J, Liu JC, Perciani CT, Ma XZ, Thoeni C, Slyper M, Eraslan G, Segerstolpe A, Manuel J, et al. (2022). Single-cell, single-nucleus, and spatial RNA sequencing of the human liver identifies cholangiocyte and mesenchymal heterogeneity. Hepatol. Commun 6, 821–840. 10.1002/hep4.1854. [PubMed: 34792289]
10. Ben-Moshe S, Veg T, Manco R, Dan S, Papinutti D, Lifshitz A, Kolodziejczyk AA, Bahar Halpern K, Elinav E, and Itzkovitz S (2022). The spatiotemporal program of zonal liver regeneration following acute injury. Cell Stem Cell 29, 973–989.e10. 10.1016/j.stem.2022.04.008. [PubMed: 35659879]
11. Pepe-Mooney BJ, Dill MT, Alemany A, Ordovas-Montanes J, Matsushita Y, Rao A, Sen A, Miyazaki M, Anakk S, Dawson PA, et al. (2019). Single-cell analysis of the liver epithelium reveals dynamic heterogeneity and an essential role for YAP in homeostasis and regeneration. Cell Stem Cell 25, 23–38.e8. 10.1016/j.stem.2019.04.004. [PubMed: 31080134]

12. Walesky CM, Kolb KE, Winston CL, Henderson J, Kruft B, Fleming I, Ko S, Monga SP, Mueller F, Apte U, et al. (2020). Functional compensation precedes recovery of tissue mass following acute liver injury. Nat. Commun 11, 5785. 10.1038/s41467-020-19558-3. [PubMed: 33214549]
13. Wang H, Zheng S, Jiang H, Wang X, Zhou F, and Weng Z (2022). Single-cell transcriptomic analysis reveals a novel cell state and switching genes during hepatic stellate cell activation in vitro. J. Transl. Med 20, 53. 10.1186/s12967-022-03263-4. [PubMed: 35093101]
14. Wang Z-Y, Keogh A, Waldt A, Cuttat R, Neri M, Zhu S, Schuierer S, Ruchti A, Crochemore C, Knehr J, et al. (2021). Single-cell and bulk transcriptomics of the liver reveals potential targets of NASH with fibrosis. Sci. Rep 11, 19396. 10.1038/s41598-021-98806-y. [PubMed: 34588551]
15. Xiong X, Kuang H, Ansari S, Liu T, Gong J, Wang S, Zhao X-Y, Ji Y, Li C, Guo L, et al. (2019). Landscape of intercellular crosstalk in healthy and NASH liver revealed by single-cell secretome gene analysis. Mol. Cell 75, 644–660.e5. 10.1016/j.molcel.2019.07.028. [PubMed: 31398325]
16. Wen Y, Lambrecht J, Ju C, and Tacke F (2021). Hepatic macrophages in liver homeostasis and diseases-diversity, plasticity and therapeutic opportunities. Cell. Mol. Immunol 18, 45–56. 10.1038/s41423-020-00558-8. [PubMed: 33041338]
17. Zigmond E, Samia-Grinberg S, Pasmanik-Chor M, Brazowski E, Shibolet O, Halpern Z, and Varol C (2014). Infiltrating monocyte-derived macrophages and resident kupffer cells display different ontogeny and functions in acute liver injury. J. Immunol 193, 344–353. 10.4049/jimmunol.1400574. [PubMed: 24890723]
18. Lawson JA, Farhood A, Hopper RD, Bajt ML, and Jaeschke H (2000). The hepatic inflammatory response after acetaminophen overdose: role of neutrophils. Toxicol. Sci 54, 509–516. 10.1093/toxsci/54.2.509. [PubMed: 10774834]
19. Liu K, Wang F-S, and Xu R (2021). Neutrophils in liver diseases: pathogenesis and therapeutic targets. Cell. Mol. Immunol 18, 38–44. 10.1038/s41423-020-00560-0. [PubMed: 33159158]
20. Jin S, Guerrero-Juarez CF, Zhang L, Chang I, Ramos R, Kuan C-H, Myung P, Plikus MV, and Nie Q (2021). Inference and analysis of cell-cell communication using CellChat. Nat. Commun 12, 1088. 10.1038/s41467-021-21246-9. [PubMed: 33597522]
21. Browaeys R, Saelens W, and Saeys Y (2020). NicheNet: modeling intercellular communication by linking ligands to target genes. Nat. Methods 17, 159–162. 10.1038/s41592-019-0667-5. [PubMed: 31819264]
22. Wang Y, Feng D, Wang H, Xu M-J, Park O, Li Y, and Gao B (2014). STAT4 knockout mice are more susceptible to concanavalin A–induced T-cell hepatitis. Am. J. Pathol 184, 1785–1794. 10.1016/j.ajpath.2014.02.023. [PubMed: 24731448]
23. Tsuda M, Zhang W, Yang G-X, Tsuneyama K, Ando Y, Kawata K, Park O, Leung PSC, Coppel RL, Ansari AA, et al. (2013). Deletion of interleukin (IL)-12p35 induces liver fibrosis in dominant-negative TGFβ receptor type II mice. Hepatology 57, 806–816. 10.1002/hep.25829. [PubMed: 22576253]
24. Knockaert L, Berson A, Ribault C, Prost P-E, Fautrel A, Pajaud J, Lepage S, Lucas-Clerc C, Bégué JM, Fromenty B, and Robin MA (2012). Carbon tetrachloride-mediated lipid peroxidation induces early mitochondrial alterations in mouse liver. Lab. Invest 92, 396–410. 10.1038/labinvest.2011.193. [PubMed: 22157718]
25. Vignali DAA, and Kuchroo VK (2012). IL-12 family cytokines: immunological playmakers. Nat. Immunol 13, 722–728. 10.1038/ni.2366. [PubMed: 22814351]
26. Trinchieri G (2003). Interleukin-12 and the regulation of innate resistance and adaptive immunity. Nat. Rev. Immunol 3, 133–146. 10.1038/nri1001. [PubMed: 12563297]
27. Reinhardt RL, Hong S, Kang S-J, Wang Z.e., and Locksley RM (2006). Visualization of IL-12/23p40 in vivo reveals immunostimulatory dendritic cell migrants that promote Th1 differentiation. J. Immunol 177, 1618–1627. 10.4049/jimmunol.177.3.1618. [PubMed: 16849470]
28. Cabeza-Cabrerizo M, Cardoso A, Minutti CM, Pereira da Costa M, and Reis e Sousa C (2021). Dendritic cells revisited. Annu. Rev. Immunol 39, 131–166. 10.1146/annurev-immunol-061020-053707. [PubMed: 33481643]
29. Yamazaki C, Sugiyama M, Ohta T, Hemmi H, Hamada E, Sasaki I, Fukuda Y, Yano T, Nobuoka M, Hirashima T, et al. (2013). Critical roles of a dendritic cell subset expressing a chemokine receptor. J. Immunol 190, 6071–6082. 10.4049/jimmunol.1202798. [PubMed: 23670193]

30. Riggan L, Hildreth AD, Rolot M, Wong YY, Satyadi W, Sun R, Huerta C, and O'Sullivan TE (2020). CRISPR-Cas9 ribonucleoprotein-mediated genomic editing in mature primary innate immune cells. Cell Rep. 31, 107651. 10.1016/j.celrep.2020.107651. [PubMed: 32433960]

31. Nabekura T, Riggan L, Hildreth AD, O'Sullivan TE, and Shibuya A (2020). Type 1 innate lymphoid cells protect mice from acute liver injury via interferon-γ secretion for upregulating bcl-xL expression in hepatocytes. Immunity 52, 96–108.e9. 10.1016/j.immuni.2019.11.004. [PubMed: 31810881]

32. Bernink JH, Peters CP, Munneke M, te Velde AA, Meijer SL, Weijer K, Hreggvidsdottir HS, Heinsbroek SE, Legrand N, Buskens CJ, et al. (2013). Human type 1 innate lymphoid cells accumulate in inflamed mucosal tissues. Nat. Immunol 14, 221–229. 10.1038/ni.2534. [PubMed: 23334791]

33. Klose CSN, Flach M, Möhle L, Rogell L, Hoyler T, Ebert K, Fabiunke C, Pfeifer D, Sexl V, Fonseca-Pereira D, et al. (2014). Differentiation of type 1 ILCs from a common progenitor to all helper-like innate lymphoid cell lineages. Cell 157, 340–356. 10.1016/j.cell.2014.03.030. [PubMed: 24725403]

34. O'Sullivan TE, Rapp M, Fan X, Weizman O-E, Bhardwaj P, Adams NM, Walzer T, Dannenberg AJ, and Sun JC (2016). Adipose-resident group 1 innate lymphoid cells promote obesity-associated insulin resistance. Immunity 45, 428–441. 10.1016/j.immuni.2016.06.016. [PubMed: 27496734]

35. Weizman O-E, Adams NM, Schuster IS, Krishna C, Pritykin Y, Lau C, Degli-Esposti MA, Leslie CS, Sun JC, and O'Sullivan TE (2017). ILC1 confer early host protection at initial sites of viral infection. Cell 171, 795–808.e12. 10.1016/j.cell.2017.09.052. [PubMed: 29056343]

36. Friedrich C, Taggenbrock RLRE, Doucet-Ladevèze R, Golda G, Moenius R, Arampatzi P, Kragten NAM, Kreymborg K, Gomez de Agüero M, Kastenmüller W, et al. (2021). Effector differentiation downstream of lineage commitment in ILC1s is driven by Hobit across tissues. Nat. Immunol 22, 1256–1267. 10.1038/s41590-021-01013-0. [PubMed: 34462601]

37. Weizman O-E, Song E, Adams NM, Hildreth AD, Riggan L, Krishna C, Aguilar OA, Leslie CS, Carlyle JR, Sun JC, and O'Sullivan TE (2019). Mouse cytomegalovirus-experienced ILC1s acquire a memory response dependent on the viral glycoprotein m12. Nat. Immunol 20, 1004–1011. 10.1038/s41590-019-0430-1. [PubMed: 31263280]

38. Garris CS, Arlauckas SP, Kohler RH, Trefny MP, Garren S, Piot C, Engblom C, Pfirschke C, Siwicki M, Gungabeesoon J, et al. (2018). Successful anti-PD-1 cancer immunotherapy requires T cell-dendritic cell crosstalk involving the cytokines IFN-γ and IL-12. Immunity 49, 1148–1161.e7. 10.1016/j.immuni.2018.09.024. [PubMed: 30552023]

39. Liu T, Zhang L, Joo D, and Sun S-C (2017). NF-κB signaling in inflammation. Signal Transduct. Target. Ther 2, 17023. 10.1038/sigtrans.2017.23. [PubMed: 29158945]

40. Harapas CR, Idiiatullina E, Al-Azab M, Hrovat-Schaale K, Reygaerts T, Steiner A, Laohamonthonkul P, Davidson S, Yu C-H, Booty L, and Masters SL (2022). Organellar homeostasis and innate immune sensing. Nat. Rev. Immunol 22, 535–549. 10.1038/s41577-022-00682-8. [PubMed: 35197578]

41. Hildreth AD, Riggan L, and O'Sullivan TE (2020). CRISPR-Cas9 ribonucleoprotein-mediated genomic editing in primary innate immune cells. STAR Protoc. 1, 100113. 10.1016/j.xpro.2020.100113. [PubMed: 33377009]

42. Hopfner K-P, and Hornung V (2020). Molecular mechanisms and cellular functions of cGAS–STING signalling. Nat. Rev. Mol. Cell Biol 21, 501–521. 10.1038/s41580-020-0244-x. [PubMed: 32424334]

43. Carozza JA, Böhnert V, Nguyen KC, Skariah G, Shaw KE, Brown JA, Rafat M, von Eyben R, Graves EE, Glenn JS, et al. (2020). Extracellular cGAMP is a cancer-cell-produced immunotransmitter involved in radiation-induced anticancer immunity. Nat. Can. (Que.) 1, 184–196. 10.1038/s43018-020-0028-4.

44. Li T, Cheng H, Yuan H, Xu Q, Shu C, Zhang Y, Xu P, Tan J, Rui Y, Li P, and Tan X (2016). Antitumor activity of cGAMP via stimulation of cGAS-cGAMP-STING-IRF3 mediated innate immune response. Sci. Rep 6, 19049. 10.1038/srep19049. [PubMed: 26754564]

45. Marcus A, Mao AJ, Lensink-Vasan M, Wang L, Vance RE, and Raulet DH (2018). Tumor-derived cGAMP triggers a STING-mediated Interferon response in non-tumor cells to activate the NK cell response. Immunity 49, 754–763.e4. 10.1016/j.immuni.2018.09.016. [PubMed: 30332631]
46. Ritchie C, Cordova AF, Hess GT, Bassik MC, and Li L (2019). SLC19A1 is an importer of the immunotransmitter cGAMP. Mol. Cell 75, 372–381.e5. 10.1016/j.molcel.2019.05.006. [PubMed: 31126740]
47. Perugorria MJ, Esparza-Baquer A, Oakley F, Labiano I, Korosec A, Jais A, Mann J, Tiniakos D, Santos-Laso A, Arbelaiz A, et al. (2019). Non-parenchymal TREM-2 protects the liver from immune-mediated hepatocellular damage. Gut 68, 533–546. 10.1136/gutjnl-2017-314107. [PubMed: 29374630]
48. Remmerie A, Martens L, Thoné T, Castoldi A, Seurinck R, Pavie B, Roels J, Vanneste B, De Prijck S, Vanhockerhout M, et al. (2020). Osteopontin expression identifies a subset of recruited macrophages distinct from kupffer cells in the fatty liver. Immunity 53, 641–657.e14. 10.1016/j.immuni.2020.08.004. [PubMed: 32888418]
49. Duarte S, Baber J, Fujii T, and Coito AJ (2015). Matrix metalloproteinases in liver injury, repair and fibrosis. Matrix Biol. 44–46, 147–156. 10.1016/j.matbio.2015.01.004.
50. Iredale JP, Benyon RC, Pickering J, McCullen M, Northrop M, Pawley S, Hovell C, and Arthur MJ (1998). Mechanisms of spontaneous resolution of rat liver fibrosis. Hepatic stellate cell apoptosis and reduced hepatic expression of metalloproteinase inhibitors. J. Clin. Invest 102, 538–549. 10.1172/JCI1018. [PubMed: 9691091]
51. Fallowfield JA, Mizuno M, Kendall TJ, Constandinou CM, Benyon RC, Duffield JS, and Iredale JP (2007). Scar-associated macrophages are a major source of hepatic matrix metalloproteinase-13 and facilitate the resolution of murine hepatic fibrosis. J. Immunol 178, 5288–5295. 10.4049/jimmunol.178.8.5288. [PubMed: 17404313]
52. Gujral JS, Liu J, Farhood A, Hinson JA, and Jaeschke H (2004). Functional importance of ICAM-1 in the mechanism of neutrophil-induced liver injury in bile duct-ligated mice. Am. J. Physiol. Gastrointest. Liver Physiol 286, G499–G507. 10.1152/ajpgi.00318.2003. [PubMed: 14563671]
53. Kono H, Uesugi T, Froh M, Rusyn I, Bradford BU, and Thurman RG (2001). ICAM-1 is involved in the mechanism of alcohol-induced liver injury: studies with knockout mice. Am. J. Physiol. Gastrointest. Liver Physiol 280, G1289–G1295. 10.1152/ajpgi.2001.280.6G1289.. [PubMed: 11352823]
54. Zhang C, Feng J, Du J, Zhuo Z, Yang S, Zhang W, Wang W, Zhang S, Iwakura Y, Meng G, et al. (2018). Macrophage-derived IL-1α promotes sterile inflammation in a mouse model of acetaminophen hepatotoxicity. Cell. Mol. Immunol 15, 973–982. 10.1038/cmi.2017.22. [PubMed: 28504245]
55. Bachmann M, Pfeilschifter J, and Mühl H (2018). A prominent role of interleukin-18 in acetaminophen-induced liver injury advocates its blockage for therapy of hepatic necroinflammation. Front. Immunol 9, 161. 10.3389/fimmu.2018.00161. [PubMed: 29472923]
56. Imaeda AB, Watanabe A, Sohail MA, Mahmood S, Mohamadnejad M, Sutterwala FS, Flavell RA, and Mehal WZ (2009). Acetaminophen-induced hepatotoxicity in mice is dependent on Tlr9 and the Nalp3 inflammasome. J. Clin. Invest 119, 305–314. 10.1172/JCI35958. [PubMed: 19164858]
57. Huang G, Besner GE, and Brigstock DR (2012). Heparin-binding epidermal growth factor-like growth factor suppresses experimental liver fibrosis in mice. Lab. Invest 92, 703–712. 10.1038/labinvest.2012.3. [PubMed: 22330337]
58. Aarts S, Reiche M, den Toom M, Gijbels M, Beckers L, Gerdes N, and Lutgens E (2019). Depletion of CD40 on CD11c+ cells worsens the metabolic syndrome and ameliorates hepatic inflammation during NASH. Sci. Rep 9, 14702. 10.1038/s41598-019-50976-6. [PubMed: 31604965]
59. Henning JR, Graffeo CS, Rehman A, Fallon NC, Zambirinis CP, Ochi A, Barilla R, Jamal M, Deutsch M, Greco S, et al. (2013). Dendritic cells limit fibroinflammatory injury in nonalcoholic steatohepatitis in mice. Hepatology 58, 589–602. 10.1002/hep.26267. [PubMed: 23322710]
60. Jiao J, Sastre D, Fiel MI, Lee UE, Ghiassi-Nejad Z, Ginhoux F, Vivier E, Friedman SL, Merad M, and Aloman C (2012). Dendritic cell regulation of carbon tetrachloride-induced murine liver fibrosis regression. Hepatology 55, 244–255. 10.1002/hep.24621. [PubMed: 21898476]

61. Heier E-C, Meier A, Julich-Haertel H, Djudjaj S, Rau M, Tschernig T, Geier A, Boor P, Lammert F, and Lukacs-Kornek V (2017). Murine CD103 + dendritic cells protect against steatosis progression towards steatohepatitis. J. Hepatol 66, 1241–1250. 10.1016/j.jhep.2017.01.008. [PubMed: 28108233]

62. Robinette ML, Fuchs A, Cortez VS, Lee JS, Wang Y, Durum SK, Gilfillan S, and Colonna MImmunological Genome Consortium; the Immunological Genome Consortium (2015). Transcriptional programs define molecular characteristics of innate lymphoid cell classes and subsets. Nat. Immunol 16, 306–317. 10.1038/ni.3094. [PubMed: 25621825]

63. Lee W, Kim HS, Hwang SS, and Lee GR (2017). The transcription factor Batf3 inhibits the differentiation of regulatory T cells in the periphery. Exp. Mol. Med 49, e393. 10.1038/emm.2017.157. [PubMed: 29147008]

64. Ataide MA, Komander K, Knöpper K, Peters AE, Wu H, Eickhoff S, Gogishvili T, Weber J, Grafen A, Kallies A, et al. (2020). BATF3 programs CD8+ T cell memory. Nat. Immunol 21, 1397–1407. 10.1038/s41590-020-0786-2. [PubMed: 32989328]

65. Deczkowska A, David E, Ramadori P, Pfister D, Safran M, Cohen M, Li B, Giladi A, Jaitin DA, Barboy O, et al. (2021). XCR1+ type 1 conventional dendritic cells drive liver pathology in non-alcoholic steatohepatitis. Nat. Med 27, 1043–1054. 10.1038/s41591-021-01344-3. [PubMed: 34017133]

66. Connolly MK, Bedrosian AS, Mallen-St Clair J, Mitchell AP, Ibrahim J, Stroud A, Pachter HL, Bar-Sagi D, Frey AB, and Miller G (2009). In liver fibrosis, dendritic cells govern hepatic inflammation in mice via TNF-α. J. Clin. Invest 119, 3213–3225. 10.1172/JCI37581. [PubMed: 19855130]

67. Gil-Farina I, Di Scala M, Salido E, López-Franco E, Rodríguez-García E, Blasi M, Merino J, Aldabe R, Prieto J, and Gonzalez-Aseguinolaza G (2016). Transient expression of transgenic IL-12 in mouse liver triggers unremitting inflammation mimicking human autoimmune hepatitis. J. Immunol 197, 2145–2156. 10.4049/jimmunol.1600228. [PubMed: 27511737]

68. Ishida Y, Kondo T, Ohshima T, Fujiwara H, Iwakura Y, and Mukaida N (2002). A pivotal involvement of IFN-γ in the pathogenesis of acetaminophen-induced acute liver injury. Faseb. J 16, 1227–1236. 10.1096/fj.02-0046com. [PubMed: 12153990]

69. Knight B, Lim R, Yeoh GC, and Olynyk JK (2007). Interferon-γ exacerbates liver damage, the hepatic progenitor cell response and fibrosis in a mouse model of chronic liver injury. J. Hepatol 47, 826–833. 10.1016/j.jhep.2007.06.022. [PubMed: 17923165]

70. Vinish M, Cui W, Stafford E, Bae L, Hawkins H, Cox R, and Toliver-Kinsky T (2016). Dendritic cells modulate burn wound healing by enhancing early proliferation: dendritic cells in wound healing. Wound Repair Regen. 24, 6–13. 10.1111/wrr.12388. [PubMed: 26609910]

71. Chen Q, Sun L, and Chen ZJ (2016). Regulation and function of the cGAS–STING pathway of cytosolic DNA sensing. Nat. Immunol 17, 1142–1149. 10.1038/ni.3558. [PubMed: 27648547]

72. Deng L, Liang H, Xu M, Yang X, Burnette B, Arina A, Li X-D, Mauceri H, Beckett M, Darga T, et al. (2014). STING-dependent cytosolic DNA sensing promotes radiation-induced type I interferon-dependent antitumor immunity in immunogenic tumors. Immunity 41, 843–852. 10.1016/j.immuni.2014.10.019. [PubMed: 25517616]

73. Klarquist J, Hennies CM, Lehn MA, Reboulet RA, Feau S, and Janssen EM (2014). STING-mediated DNA sensing promotes antitumor and autoimmune responses to dying cells. J. Immunol 193, 6124–6134. 10.4049/jimmunol.1401869. [PubMed: 25385820]

74. Woo S-R, Fuertes MB, Corrales L, Spranger S, Furdyna MJ, Leung MYK, Duggan R, Wang Y, Barber GN, Fitzgerald KA, et al. (2014). STING-dependent cytosolic DNA sensing mediates innate immune recognition of immunogenic tumors. Immunity 41, 830–842. 10.1016/j.immuni.2014.10.017. [PubMed: 25517615]

75. An P, Wei L-L, Zhao S, Sverdlov DY, Vaid KA, Miyamoto M, Kuramitsu K, Lai M, and Popov YV (2020). Hepatocyte mitochondria-derived danger signals directly activate hepatic stellate cells and drive progression of liver fibrosis. Nat. Commun 11, 2362. 10.1038/s41467-020-16092-0. [PubMed: 32398673]

76. Araujo A, Antunes M, Mattos M, Diniz A, Alvarenga D, Nakagaki B, Carvalho É, Lacerda V, Carvalho-Gontijo R, Goulart J, et al. (2018). Liver immune cells release type 1 Interferon

due to DNA sensing and amplify liver injury from acetaminophen overdose. Cells 7, 88. 10.3390/cells7080088. [PubMed: 30060463]

77. Marques PE, Oliveira AG, Pereira RV, David BA, Gomides LF, Saraiva AM, Pires DA, Novaes JT, Patricio DO, Cisalpino D, et al. (2015). Hepatic DNA deposition drives drug-induced liver injury and inflammation in mice: marques, oliveira, et al. Hepatology 61, 348–360. 10.1002/hep.27216. [PubMed: 24824608]
78. Wang T, Yu H, Hughes NW, Liu B, Kendirli A, Klein K, Chen WW, Lander ES, and Sabatini DM (2017). Gene essentiality profiling reveals gene networks and synthetic lethal interactions with oncogenic ras. Cell 168, 890–903.e15. 10.1016/j.cell.2017.01.013. [PubMed: 28162770]
79. Butler A, Hoffman P, Smibert P, Papalexi E, and Satija R (2018). Integrating single-cell transcriptomic data across different conditions, technologies, and species. Nat. Biotechnol 36, 411–420. 10.1038/nbt.4096. [PubMed: 29608179]
80. Bankhead P, Loughrey MB, Fernández JA, Dombrowski Y, McArt DG, Dunne PD, McQuaid S, Gray RT, Murray LJ, Coleman HG, et al. (2017). QuPath: open source software for digital pathology image analysis. Sci. Rep 7, 16878. 10.1038/s41598-017-17204-5. [PubMed: 29203879]
81. Mayer CT, Ghorbani P, Nandan A, Dudek M, Arnold-Schrauf C, Hesse C, Berod L, Stüve P, Puttur F, Merad M, and Sparwasser T (2014). Selective and efficient generation of functional Batf3-dependent CD103+ dendritic cells from mouse bone marrow. Blood 124, 3081–3091. 10.1182/blood-2013-12-545772. [PubMed: 25100743]
82. Daemen S, Gainullina A, Kalugotla G, He L, Chan MM, Beals JW, Liss KH, Klein S, Feldstein AE, Finck BN, et al. (2021). Dynamic shifts in the composition of resident and recruited macrophages influence tissue remodeling in NASH. Cell Rep. 34, 108626. 10.1016/j.celrep.2020.108626. [PubMed: 33440159]

Highlights

- *Il12b* is a regulator of acute liver injury-induced changes in gene expression *in silico*
- cDC1-derived IL-12 signaling protects against acute liver injury
- cDC1-derived IL-12 induces protective liver-resident ILC1 IFN-γ responses
- cDC1-intrinsic cGAS-STING signaling is required for IL-12 production

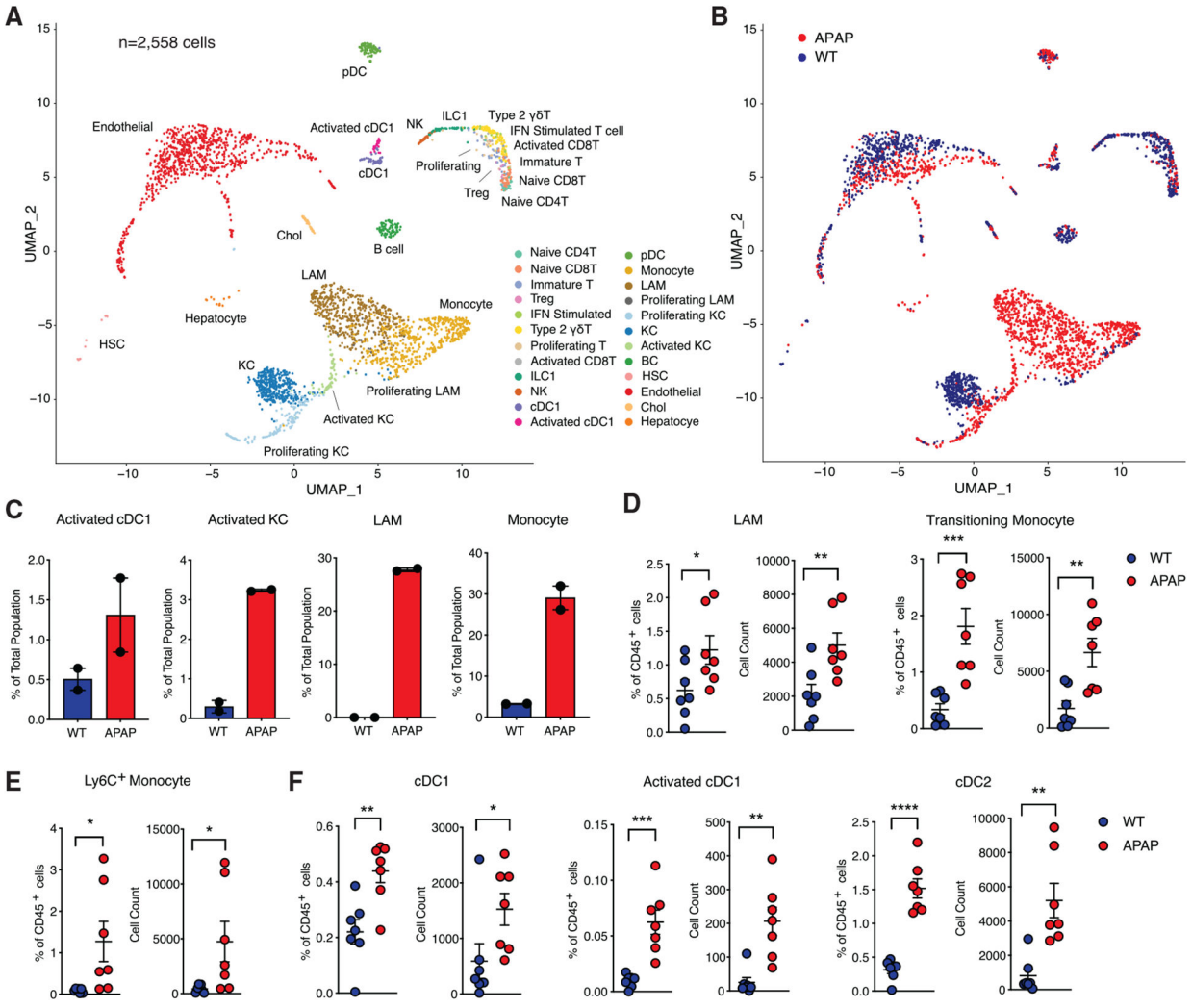

Figure 1. scRNA-seq analysis of APAP-induced liver injury identifies early activation states of liver-resident immune cells

(A) Uniform manifold approximation and projection (UMAP) plot of 2,558 mouse liver cells harvested from healthy or 24 h post-acetaminophen (APAP) treatment. Cells are colored by their annotations derived from cluster-specific analysis.

(B) UMAP indicating cell source: WT (blue) or APAP treated (red).

(C) The frequencies of APAP-enriched myeloid subsets from the total WT or APAP-treated cells (n = 2 mice per cohort).

(D–F) The numbers and frequencies of (D and E) macrophage, monocyte, and (F) dendritic cell subsets from total liver $CD45^+$ cells isolated from saline-treated control (WT) or APAP-treated mice 24 h after treatment (n = 7 mice per cohort).

Data are representative of two independent experiments (D), and samples were compared using two-tailed Student's t test with Welch's correction, assuming unequal SD. Data are presented as individual points with the mean ± SEM (*p < 0.05, **p < 0.01).

See also Figure S1 and Table S1.

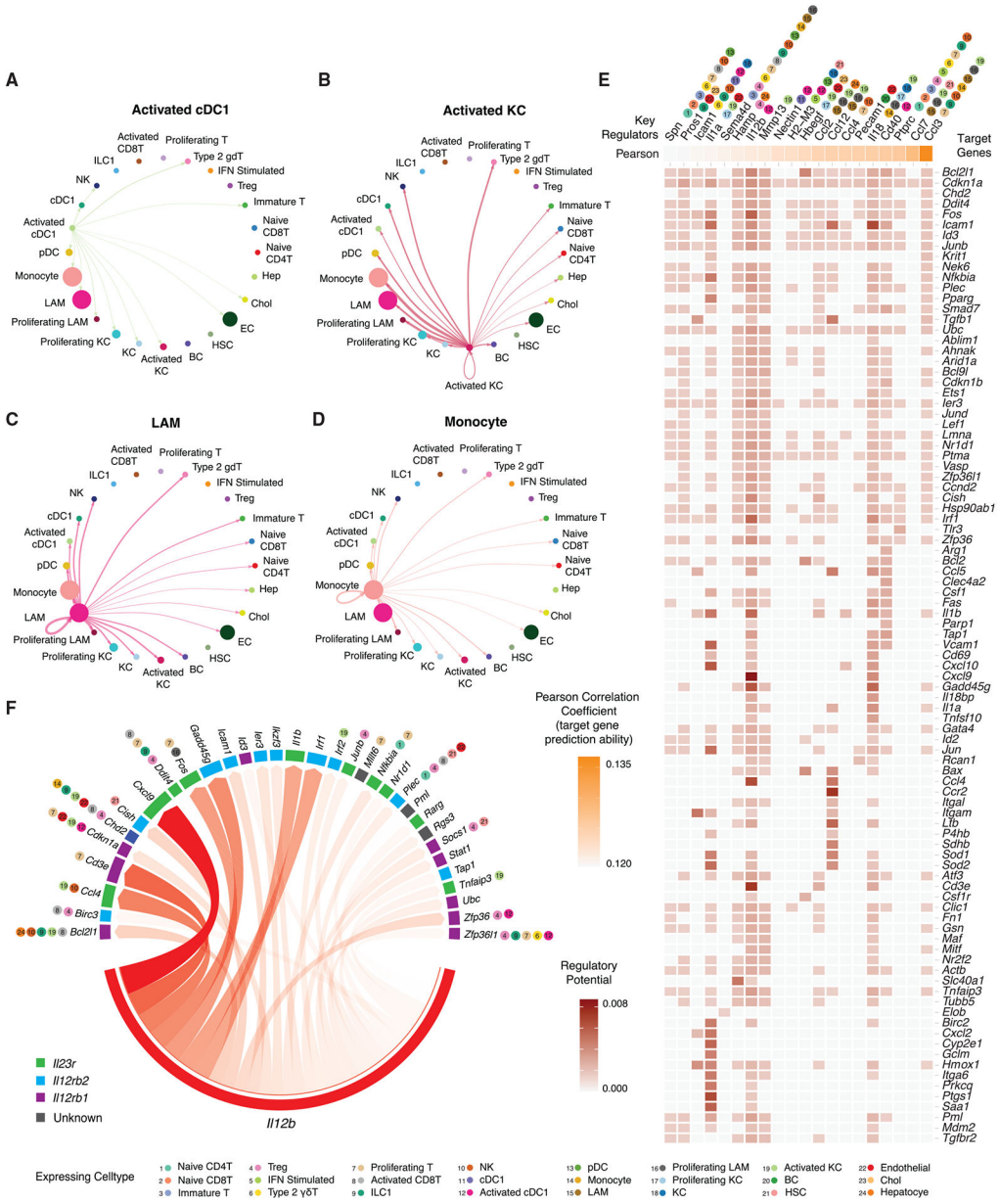

Figure 2. scRNA-seq receptor-ligand analysis identifies upstream regulators of liver injury-associated differentially expressed genes

(A–D) CellChat receptor-ligand analysis of the inferred intercellular communication networks from APAP-enriched cell states. Different cell types are represented by different colors within the circle plot. Arrows are proportional to the interaction strength between two cell types, while node size is relative to the number of cells within that population.

(A) Weighted interactions stemming from activated cDC1s.

(B) Weighted interactions from activated KCs.

(C) Weighted interactions from LAMs.

(D) Weighted interactions from monocytes.

(E) NicheNet ligand activity prediction analysis. Results are shown for the top 20 ranked key regulator ligands and their target genes of interest. The top 25% of the interaction scores

between each of these key regulators and their top 50 most strongly predicted gene targets were plotted within the regulatory potential matrix. Colored dots above the key regulators denote which cell types following APAP treatment express the ligand.

(F) NicheNet circos plot visualization of the top active ligand-target links between *Il12b* and its top-predicted target genes. Width of the target block and degree of arrow transparency are proportional to the ligand-target regulatory potential value; larger/darker indicates a higher regulatory potential. Color of the target block denotes which signal is upstream of the target: IL-23 (green), IL-12 (blue), IL-23 and IL-12 (purple), or unknown (gray). Colored dots above the predicted targets denote which cell populations within the APAP-treated dataset express the gene.

See also Figure S2 and Tables S2, S3, S4, S5, S6, and S7.

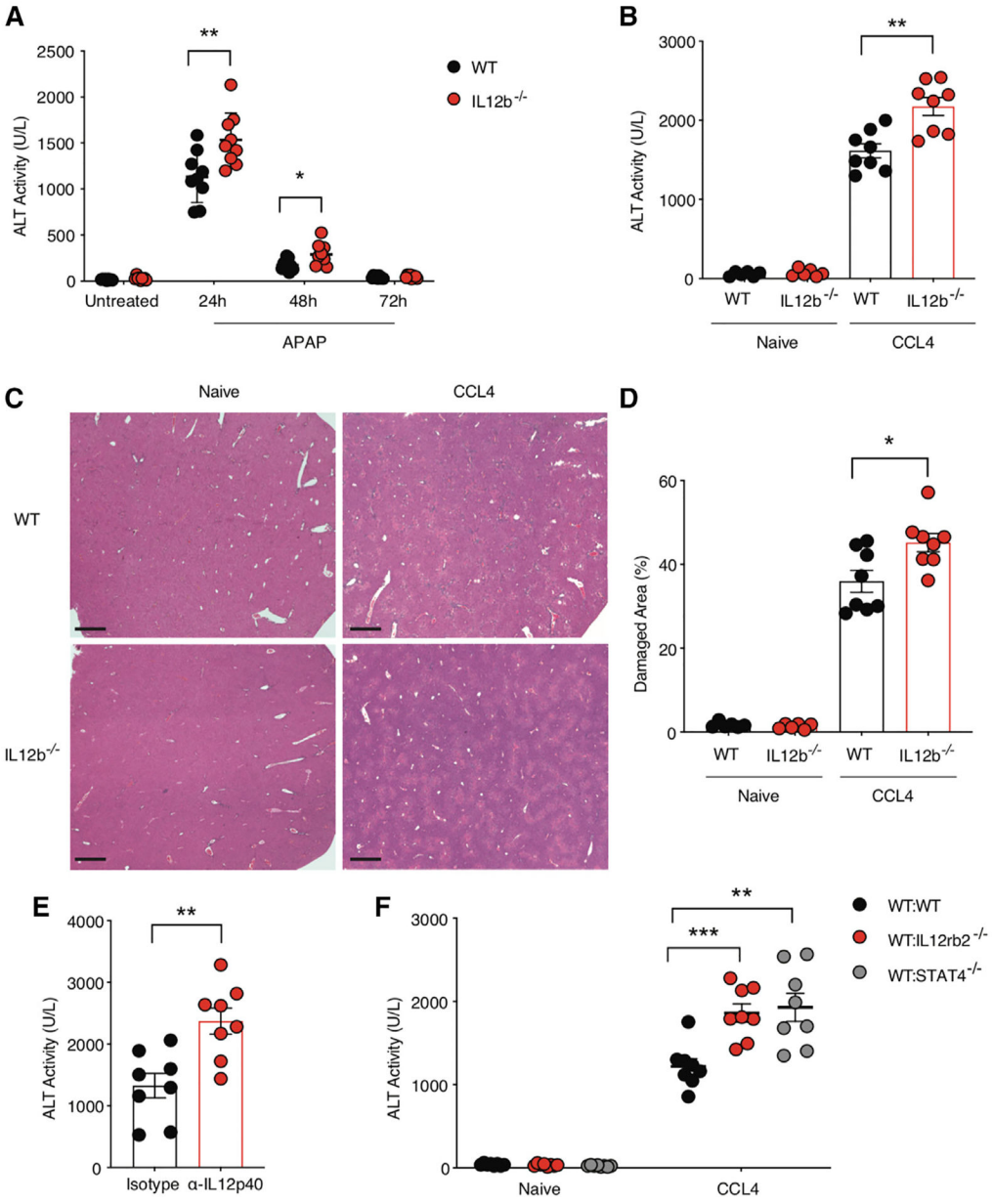

Figure 3. IL-12 signaling in hematopoietic-derived cells protects against acute liver injury

(A) Plasma ALT concentrations from WT or *IL12b*$^{-/-}$ mice before and 24, 48, and 72 h after APAP injection (n = 8 mice per group).

(B) Plasma ALT concentrations from WT or IL12b$^{-/-}$ mice before and 48 h after CCl_4 injection (n = 8 mice per group).

(C) Histology of the liver left lateral lobes (hematoxylin and eosin staining) of WT or *IL12b*$^{-/-}$ mice before and 48 h after CCl_4 injection (n = 6–8 mice per group). Scale bars represent 500 μm.

(D) Quantification of centrilobular hepatocyte necrosis and damaged areas around the central veins in the livers of WT or *IL12b*$^{-/-}$ mice before and 48 h after CCl_4 injection (n = 6–8 mice per group).

(E) Plasma ALT concentrations of mice (that had been injected with a neutralizing anti-Il12p40 mAb or isotype Ig 12 h before and 12 h after CCl_4 injection) 48 h after CCl_4 injection (n = 8 mice per cohort).

(F) Bone marrow chimeric mice were generated utilizing WT hosts reconstituted with either WT, *Il12rb2*$^{-/-}$, or *Stat4*$^{-/-}$ bone marrow. Plasma ALT concentrations of WT:WT, WT:*Il12rb2*$^{-/-}$, and WT:*Stat4*$^{-/-}$ mice before and 48 h after CCl_4 injection (n = 8 mice per group).

Data are representative of two independent experiments (A–F), and samples were compared using two-tailed Student's t test with Welch's correction, assuming unequal SD. Data are presented as individual points with the mean ± SEM (*$p < 0.05$, **$p < 0.01$, ***$p < 0.001$).

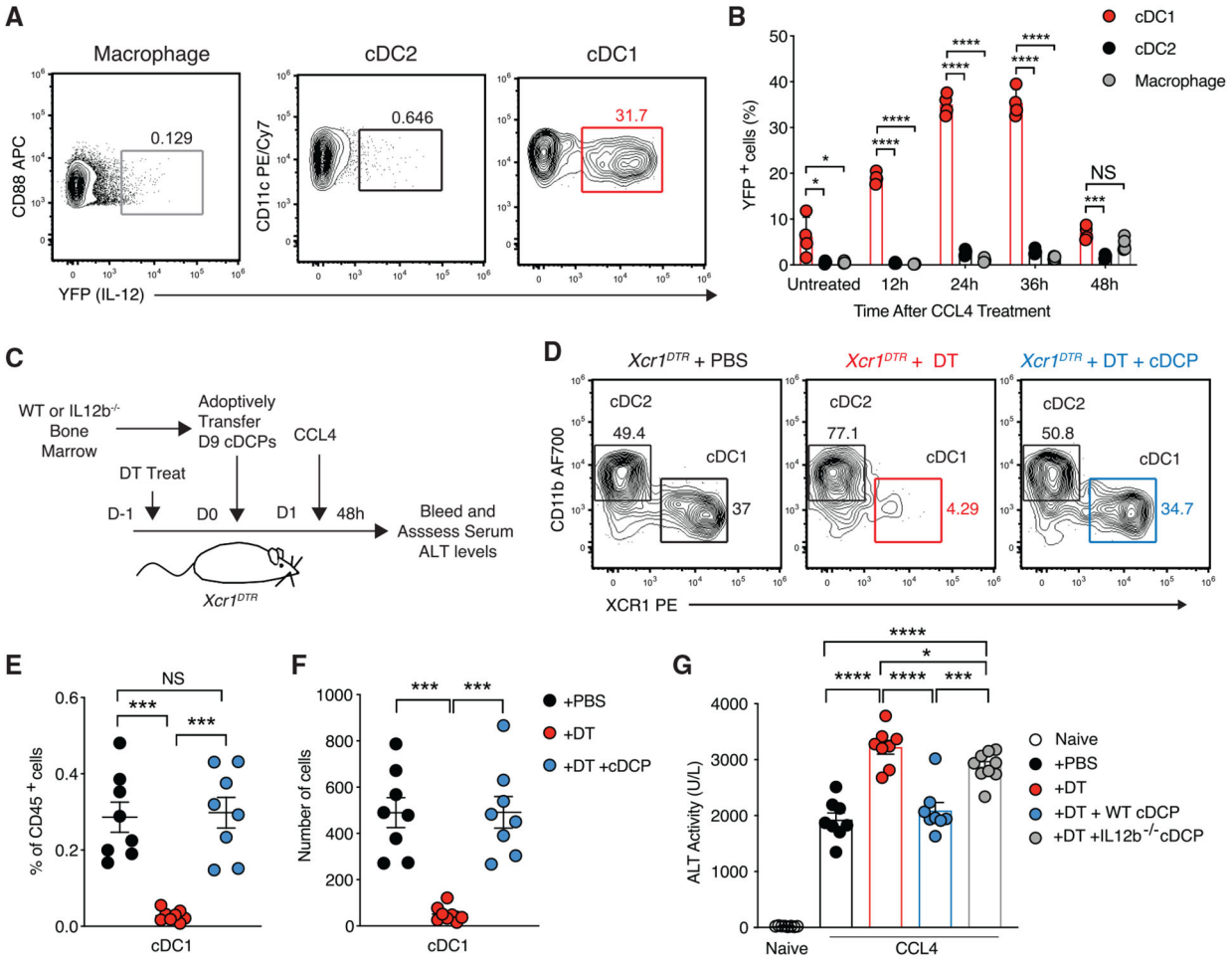

Figure 4. cDC1-derived IL-12 protects against acute liver injury

(A and B) *Il12b*^{YFP} reporter mice were either untreated or injected with CCl_4 and livers were harvested 12, 24, 36, and 48 h later to assess YFP$^+$ cells by flow cytometry.

(A) Representative flow plots of YFP$^+$ percentage within liver CD45$^+$Lin$^-$CD88$^+$ macrophage (left), CD45$^+$Lin$^-$CD88$^-$MHCII$^+$CD11c$^+$CD11b$^+$XCR1$^-$ cDC2 (middle), or CD45$^+$Lin$^-$CD88$^-$MHCII$^+$CD11c$^+$CD11b$^-$XCR1$^+$ cDC1 (right) populations 24 h after CCl_4 injection.

(B) Kinetics of the percentages of YFP$^+$ cells in macrophage, cDC2, and cDC1 populations in the liver after CCl_4 injection (n = 4 mice per group).

(C) Schematic of adoptive transfer model using *Xcr1*^{DTR} mice. Briefly, *Xcr1*^{DTR} mice were either untreated or treated with PBS, DT, or DT followed by adoptive transfer of 1 × 10^7 D9 bone marrow-derived WT cDCPs or *IL12b*$^{-/-}$ cDCPs 1 day prior to CCl_4 treatment. Mice were bled and plasma ALT concentrations were analyzed 48 h after CCl_4 injection.

(D) Representative flow plots showing liver cDC2 and cDC1 populations in *Xcr1*^{DTR} mice 24 h after PBS (left), DT (middle), or DT treatment plus adoptive transfer of bone marrow-derived cDCPs (right) (n = 8 mice per cohort).

(E) The frequencies of cDC1s from total liver CD45$^+$ cells of PBS-treated, DT-treated, or DT-treated plus adoptively transferred (+cDCP) *Xcr1*^{DTR} mice 24 h after treatment (n = 8 mice per cohort).

(F) The numbers of liver cDC1s from PBS-treated, DT-treated, or DT-treated plus adoptively transferred (+cDCP) *Xcr1*^{DTR} mice 24 h after treatment (n = 8 mice per cohort).
(G) Plasma ALT concentrations from naive, PBS-treated, DT-treated, DT-treated plus WT transferred cDCPs, or DT-treated plus *IL12b*$^{-/-}$ cDCPs *Xcr1*^{DTR} mice 48 h after CCl_4 injection (n = 8–9 mice per group).
Data are representative of three (D–F) and two independent experiments (A, B, and G), and samples were compared using two-tailed Student's t test with Welch's correction, assuming unequal SD. Data are presented as individual points with the mean ± SEM (NS, not significant, *p < 0.05, **p < 0.01, ***p < 0.001, ****p < 0.0001).
See also Figure S3.

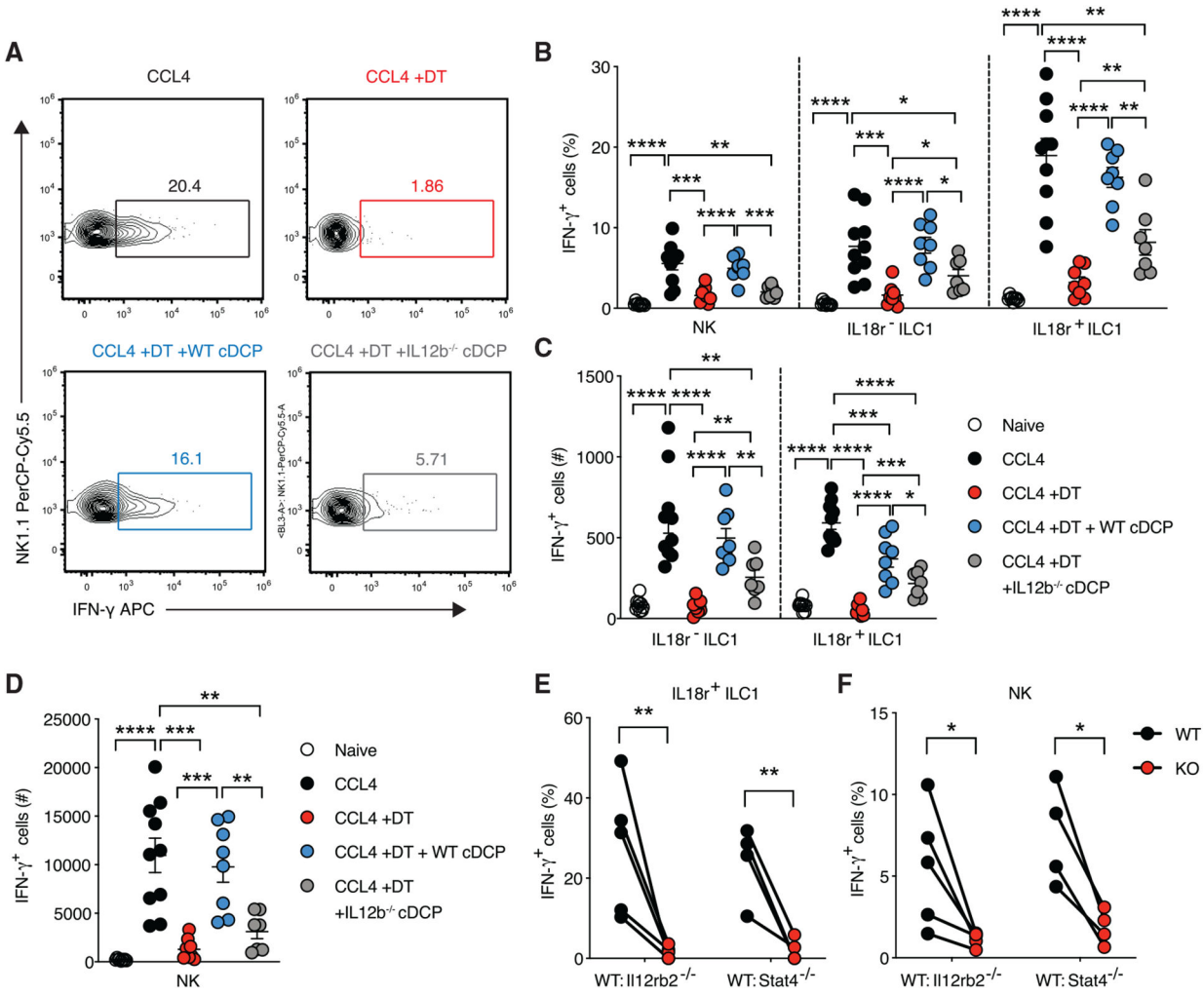

Figure 5. cDC1-derived IL-12 is required for group 1 ILC IFN-γ production following sterile liver injury

(A–D) Xcr1^{DTR} mice were untreated (naive) or CCl_4, CCl_4 + DT, CCl_4 + DT + WT transferred cDCP, or CCl_4 + DT + *IL12b*$^{-/-}$ transferred cDCP treated before group 1 ILC IFN-γ was assessed 18 h later (n = 7–10 mice per group).

(A) Representative flow plots of IFN-γ$^+$ percentage within liver CD45$^+$Lin$^-$NK1.1$^+$CD200r$^+$CD49b$^-$IL18r$^+$ ILC1 from CCl_4- (top left), CCl_4 + DT- (top right), CCl_4 + DT + WT transferred cDCP- (bottom left), or CCl_4 + DT + *IL12b*$^{-/-}$ transferred cDCP-treated (bottom right) cohorts.

(B) The percentages of IFN-γ$^+$ IL18r$^+$ ILC1s, IL18r$^-$ ILC1s, and CD45$^+$Lin$^-$NK1.1$^+$CD200r$^-$CD49b$^+$ NK cells from the indicated cohorts.

(C) The numbers of IFN-γ$^+$ IL18r$^+$ and IL18r$^-$ ILC1s.

(D) The numbers of IFN-γ$^+$ NK cells.

(E and F) Mixed bone marrow chimeric mice were generated using congenically distinct WT (CD45.1 × 2) hosts reconstituted with a 1:1 mixture of either WT (CD45.1):*Il12rb2*$^{-/-}$ (CD45.2) or WT (CD45.1):*Stat4*$^{-/-}$ (CD45.2) bone marrow. The percentages of IFN-γ$^+$ (E) IL18r$^+$ ILC1s and (F) NK cells in the liver of WT:*Il12rb2*$^{-/-}$ and WT:*Stat4*$^{-/-}$ mice were derived from either WT or knockout (KO) bone marrow (n = 4–5 mice per group).

Data are representative of two independent experiments (A–F), and samples were compared using two-tailed Student's t test with Welch's correction, assuming unequal SD. Data are presented as individual points with the mean ± SEM (NS, not significant, *p < 0.05, **p < 0.01, ***p < 0.001, ****p < 0.0001).

See also Figure S4.

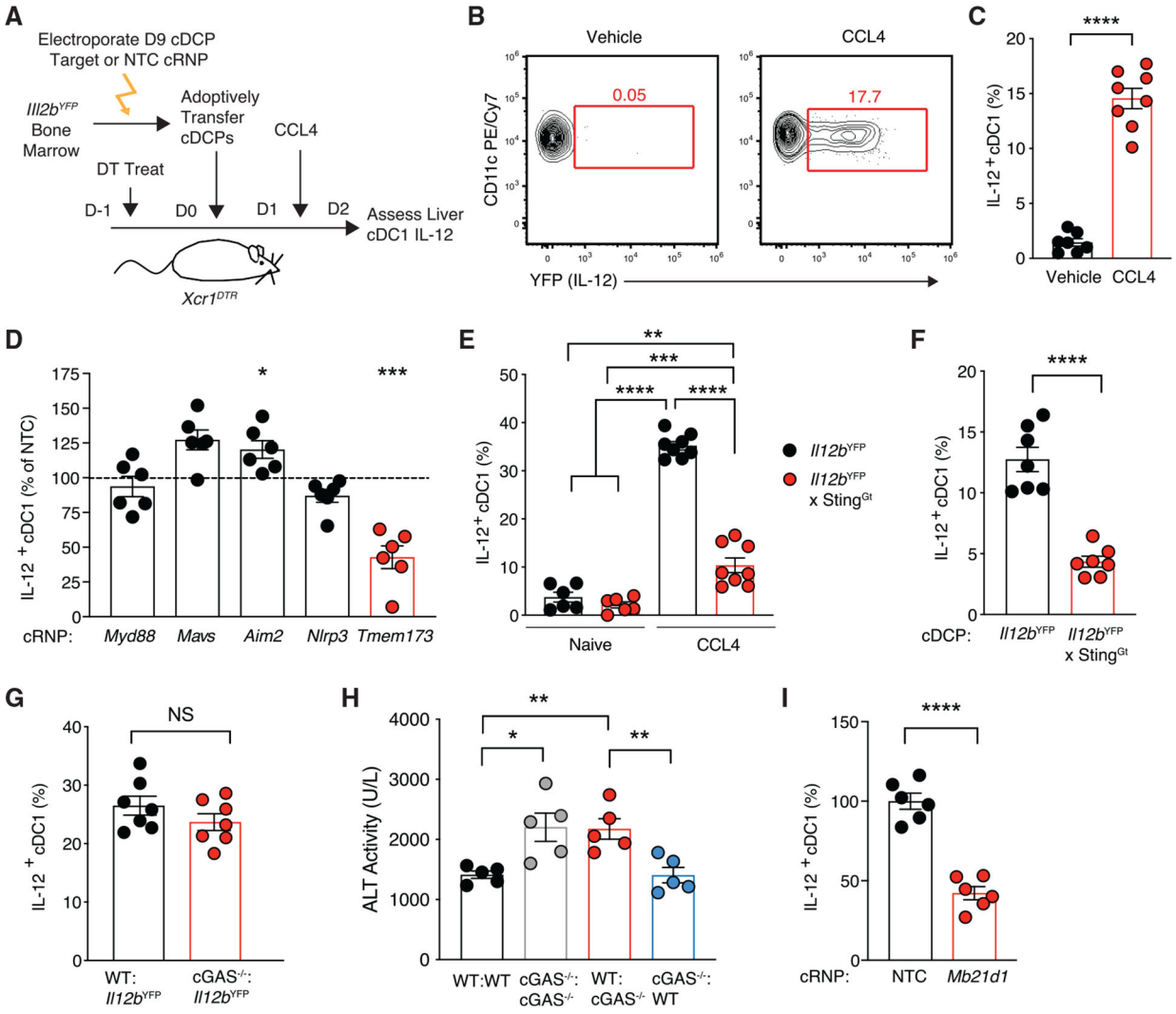

Figure 6. cGAS-STING signaling is critical for cDC1-derived IL-12 production and protective function during sterile liver injury

(A) Schematic of adoptive transfer model system using CRISPR cRNP-edited cells. Briefly, 1×10^7 *Il12b*^{YFP} bone marrow-derived cDCPs were cRNP edited against target genes or nontargeting control (NTC) before adoptive transfer into DT-treated *Xcr1*^{DTR} mice 1 day prior to CCl_4 treatment. Livers were then harvested, and the percentages of YFP$^+$ cDC1 were analyzed 24 h after CCl_4 injection.

(B and C) Unedited *Il12b*^{YFP} bone marrow-derived cDC1s were transferred into *Xcr1*^{DTR} mice 1 day prior to vehicle or CCl_4 treatment.

(B) Representative flow plots of adoptively transferred YFP$^+$ cDC1s from vehicle- (left) or CCl_4-treated (right) mouse livers 24 h after treatment.

(C) Percentages of YFP$^+$ (IL-12$^+$) from vehicle- or CCl_4-treated mouse livers 24 h after treatment (n = 7–8 mice per group).

(D) Analysis of liver IL-12$^+$ cDC1s from adoptively transferred target (*Myd88*, *Mavs*, *Aim2*, *Nlrp3*, *Tmem173* [STING]) cRNP-edited cells as a percentage of NTC-cRNP-edited cells 24 h after CCl_4 treatment (n = 6 mice per group).

(E) Percentages of IL-12$^+$ cDC1s in the liver of *Il12b*^{YFP} or *Il12b*^{YFP} × Sting^{Gt} mice before and 24 h after CCl_4 injection (n = 6–8 mice per group).
(F) Analysis of liver IL-12$^+$ cDC1s from adoptively transferred bone marrow-derived *Il12b*^{YFP} or *Il12b*^{YFP} × Sting^{Gt} cells 24 h after CCl_4 treatment (n = 7 mice per group).
(G) Bone marrow chimeric mice were generated utilizing WT or *cGAS*$^{-/-}$ hosts reconstituted with *Il12b*^{YFP} bone marrow. Percentages of liver IL-12$^+$ cDC1s from WT:*Il12b*^{YFP} or *cGAS*$^{-/-}$:*Il12b*^{YFP} mice 24 h after CCl_4 treatment (n = 7 mice per group).
(H) Bone marrow chimeric mice were generated utilizing WT or *cGAS*$^{-/-}$ hosts reconstituted with either WT or *cGAS*$^{-/-}$ bone marrow. Plasma ALT concentrations of WT (host):WT (BM), WT:*cGAS*$^{-/-}$, *cGAS*$^{-/-}$:WT, and *cGAS*$^{-/-}$:*cGAS*$^{-/-}$ mice 48 h after CCl_4 injection (n = 5 mice per group).
(I) Analysis of liver IL-12$^+$ cDC1s from adoptively transferred target (*Mb21d1* [cGAS]) cRNP-edited cells as a percentage of NTC-cRNP-edited cells 24 h after CCl_4 treatment (n = 6 mice per group).
Data are representative of three (D and I) and two (B, C, and E–H) independent experiments, and samples were compared using two-tailed Student's t test with Welch's correction, assuming unequal SD. Data are presented as individual points with the mean ± SEM (NS, not significant, *p < 0.05, **p < 0.01, ***p < 0.001, ****p < 0.0001).
See also Figure S5.

KEY RESOURCES TABLE

REAGENT or RESOURCE	SOURCE	IDENTIFIER
Antibodies		
PerCP-Cy5.5 Anti-Mouse NK1.1 (PK136)	BioLegend	Cat# 108727
APC/Cy7 Anti-Mouse NK1.1 (PK136)	BioLegend	Cat# 108723
APC/Cy7 Anti-Mouse CD3e (17A2)	BioLegend	Cat# 100222
APC/Cy7 Anti-Mouse Ly6G (1A8)	BioLegend	Cat# 127623
Pacific Blue Anti-Mouse Ly6C (HK1.4)	BioLegend	Cat# 128013
APC Anti-Mouse IFN-γ (XMG1.2)	BioLegend	Cat# 505809
Alexa Fluor 700 Anti-Mouse CD11b (M1/70)	BioLegend	Cat# 101222
Pacific Blue Anti-Mouse CD25 (PC61)	Biolegend	Cat# 102021
APC/Cy7 Anti-Mouse CD19 (6D5)	BioLegend	Cat# 115529
PE/Cy7 Anti-Mouse CD49b (DX5)	BioLegend	Cat# 108922
Pacific Blue Anti-Mouse IL-18ra (P3TUNYA)	eBioscience	Cat# 48–5183-80
Alexa Fluor 700 Anti-Mouse CD45.1 (A20)	BioLegend	Cat# 110724
FITC Anti-Mouse CD45.2 (104)	BioLegend	Cat# 109806
Pacific Blue Anti-Mouse CD45.2 (104)	BioLegend	Cat# 109819
APC/Cy7 Anti-Mouse TCRβ (H57–597)	BioLegend	Cat# 109220
PE Anti-Mouse CD200r1 (OX-110)	BioLegend	Cat# 123907
PE/Cy7 Anti-Mouse CD11c (N418)	BioLegend	Cat# 117317
PE Anti-Mouse XCR1 (ZET)	BioLegend	Cat# 148203
PerCP-Cy5.5 Anti-Mouse MHCII/I-A/I-E (M5/114.15.2)	BioLegend	Cat# 107625
APC Anti-Mouse CD88 (20/70)	BioLegend	Cat# 135808
Alexa Fluor 700 Anti-Mouse F4/80 (BM8)	BioLegend	Cat# 123129
PE/Cy7 Anti-Mouse Tim-4 (RMT4–54)	BioLegend	Cat# 130009
PE Anti-Mouse CX3CR1 (SA011F11)	BioLegend	Cat# 149005
PerCP-Cy5.5 Anti-Mouse CD9 (MZ3)	BioLegend	Cat# 124817
cGAS (D3O8O) Rabbit mAb (Mouse Specific)	Cell Signaling	Cat# 31659S
STING (D2P2F) Rabbit mAB	Cell Signaling	Cat# 13647S
AIM2 Antibody (Mouse Specific)	Cell Signaling	Cat# 63660S
NLRP3 (D4D8T) Rabbit mAb	Cell Signaling	Cat# 15101S
MAVS Antibody (Rodent Specific)	Cell Signaling	Cat# 4983S
MyD88 (D80F5) Rabbit mAb	Cell Signaling	Cat# 4283S
Goat anti-Rabbit IgG (H + L) Secondary Antibody, HRP	ThermoFisher	Cat# 31466
*In Vivo*MAb anti-mouse IL-12p40 (C17.8)	Bio X Cell	Cat# BE0051
*In Vivo*MAb rat IgG2a isotype control (2A3)	Bio X Cell	Cat# BE0089
Chemicals, peptides, and recombinant proteins		
Acetaminophen	Sigma-Aldrich	Cat# A7085
Carbon tetrachloride	Sigma-Aldrich	Cat# 289116
Corn oil	Sigma-Aldrich	Cat# C8267
Brefeldin A	BioLegend	Cat# 420601
Monensin (Golgistop)	BioLegend	Cat# 420701

REAGENT or RESOURCE	SOURCE	IDENTIFIER
Cas9-NLS	SYNTHEGO	N/A
Alt-R® Cas9 Electroporation Enhancer, 10 nmol	IDT	Cat# 1075916
Synthetic Guide RNAs	SYNTHEGO	N/A
Recombinant mouse GM-CSF	Peprotech	Cat# 315–03
Recombinant mouse FLT3-L	Peprotech	Cat# 250–31L
Percoll	VWR	Cat# 17–0891-02
Collagenase A	Sigma	Cat# 10103578001
DNase I	Sigma	Cat# 10104159001
Diphtheria toxin, Unnicked, from *Corynebacterium diphtheriae*	List Biological Laboratories	Cat# 150
Critical commercial assays		
Pointe Scientific ALT (SGPT) Liquid Reagents	Fisher Scientific	Cat# 23–666-087
Foxp3/Transcription Factor Staining kit	ThermoFisher	Cat# 00–5523-00
SuperSignal West Pico PLUS ECL kit	ThermoFisher	Cat# 34580
DNeasy Blood and Tissue kit	Qiagen	Cat# 69504
Deposited data		
single cell transcriptomics of mouse liver cells at different time points after APAP ip injection	Ben-Moshe et al.[10]	Zenodo https://doi.org/10.5281/zenodo.6035873
Experimental models: Organisms/strains		
Mouse: C57BL/6 (CD45.2)	Jackson Laboratory	Stock # 000664
Mouse: B6.SJL (CD45.1)	Jackson Laboratory	Stock #002114
Mouse: B6.129S1-*Il12b*^{tm1Jm}/J (*Il12b*$^{-/-}$)	Jackson Laboratory	Stock # 002693
Mouse: B6.129-*Il12b*$^{tm1.1Lky}$/*J* (*Il12b*^{YFP})	Jackson Laboratory	Stock #006412
Mouse: C57BL/6J-*Sting1*^{gt}/J (*Tmem173*$^{-/-}$; STING$^{-/-}$)	Jackson Laboratory	Stock #017537
Mouse: B6(C)-*Cgas*$^{tm1d(EUCOMM)Hmgu}$/J (*Mb21d1*$^{-/-}$; cGAS$^{-/-}$)	Jackson Laboratory	Stock # 026554
Mouse: *B6.129-Il12b*$^{tm1.1Lky}$/*J* C57BL/6J-*Sting1*^{gt}/J (*Il12b*^{YFP}×Sting^{Gt})	O'Sullivan (PI) Lab	N/A
Mouse: *Xcr1*$^{+/DTRvenus}$	O'Sullivan (PI) Lab	N/A
Mouse: C57BL/6J-*Stat4*^{em3Adiuj}/J (*Stat4*$^{-/-}$)	Jackson Laboratory	Stock # 028526
Mouse: B6; 129S1-*Il12rb2*^{tm1Jm}/J (*Il12rb2*$^{-/-}$)	Jackson Laboratory	Stock # 003248
Oligonucleotides		
sgRNA targeting sequence: *Rosa26* (NTC) ACTCCAGTCTTTCTAGAAGA	Riggan et al.[30]	N/A
sgRNA targeting sequence: *Tmem173* (STING) CCAGCCATCCCACGGCCCAG	Wang et al.[78]	N/A
sgRNA targeting sequence: *Myd88* GGTTCAAGAACAGCGATAGG	Wang et al.[78]	N/A
sgRNA targeting sequence: *Mb21d1* (cGAS) GGTGTGGAGCAGCTGAACAC	Wang et al.[78]	N/A
sgRNA targeting sequence: *Mavs* GCCGTCGCGAGGATGTCTGG	Wang et al.[78]	N/A
sgRNA targeting sequence: *Aim2* AAAGAAGAGAGGAACACAGA	Wang et al.[78]	N/A
sgRNA targeting sequence: *Nlrp3* CCATCGGCCGGACTAAAATG	Wang et al.[78]	N/A
sgRNA PCR Primers see Table S8	Multiple	N/A
Software and algorithms		
R 4.1.2 and R studio	R Consortium	https://www.rstudio.com/

REAGENT or RESOURCE	SOURCE	IDENTIFIER
Seurat	Butler et al.[79]	https://satijalab.org/seurat/
CellChat	Jin et al.[20]	https://github.com/sqjin/CellChat
NicheNet	Browaeys et al.[21]	https://github.com/saeyslab/nichenetr
FlowJo, Version 9.9.6	Ashland, OR: Becton, Dickinson and Company	https://www.flowjo.com/solutions/flowjo
Prism	GraphPad	https://www.graphpad.com/scientific-software/prism
ICE Analysis	SYNTHEGO	https://ice.synthego.com/
QuPath	Bankhead et al.[80]	https://qupath.github.io/
Other		
Neon Transfection System	ThermoFisher	Cat# MPK5000
Neon 100 µL transfection kit	ThermoFisher	Cat# MPK10096
Dounce Glass Tissue Homogenizer, 7mL	Wheaton	Cat# 357542
NuPage 4–12% Bis-Tris Gel, 1.0 mm × 15 well	Invitrogen	Cat# NP0323BOX
PVDF Transfer Membrane, 0.45µm, 10 cm × 10 cm	ThermoFisher	Cat# 88585
NanoDrop OneC Microvolume UV-Vis Spectrophotometer	ThermoScientific	Cat# ND-ONEC-W
Attune NxT Flow Cytometer	ThermoScientific	N/A